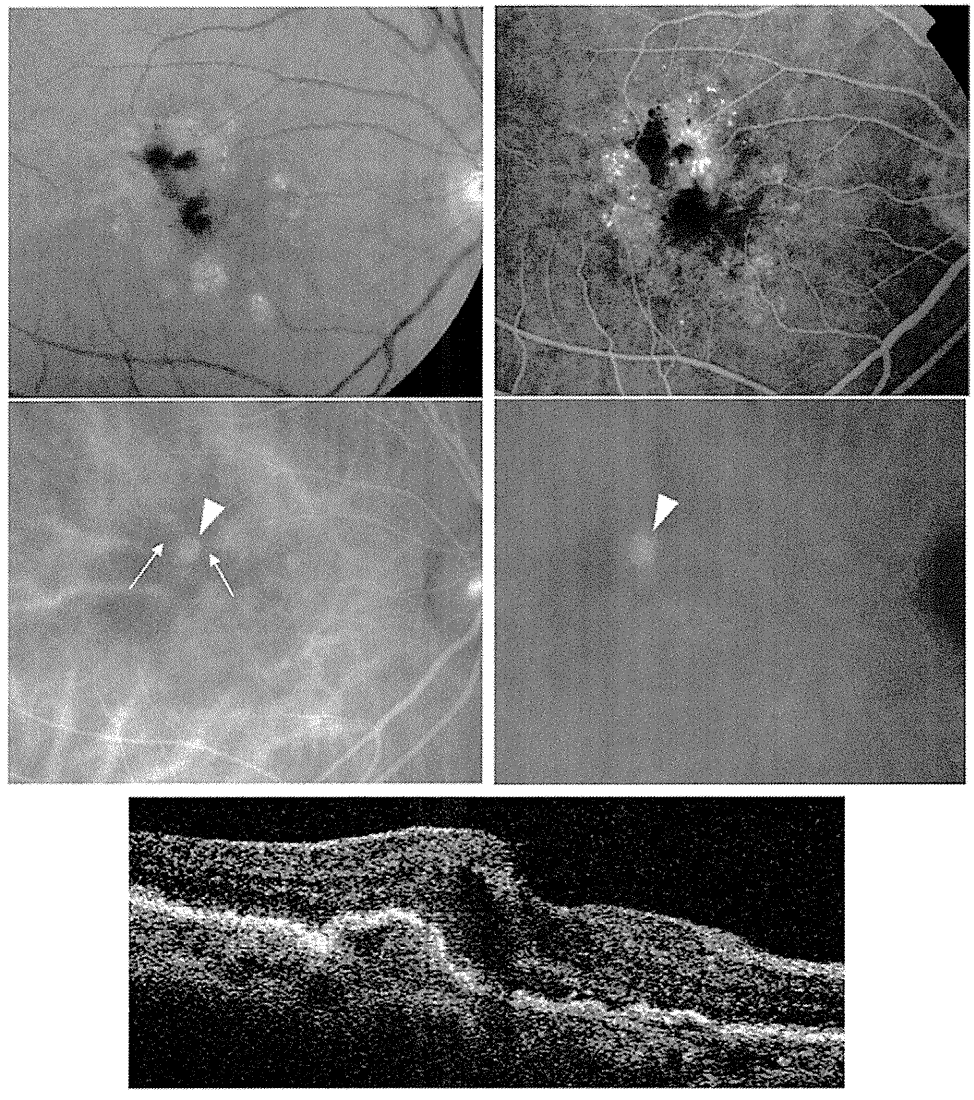

FIGURE 3. Case 7: an 84-year-old woman was treated with combined intravitreal triamcinolone acetonide with photodynamic therapy (IVTA plus PDT) for stage 2 retinal angiomatous proliferation (RAP) with a pigment epithelial detachment (PED). At baseline, the best-corrected visual acuity (BCVA) was 0.6 decimal VA in the right eye with stage 2 RAP. (Top left) Red-free photograph showing small intraretinal and preretinal hemorrhages, a PED, and drusen. (Top right) Fluorescein angiogram showing leakage and intraretinal edema. (Middle left) Early-phase indocyanine green angiogram (ICGA) showing retinal-retinal anastomosis (arrows) and a RAP lesion (arrowhead). (Middle right) Late-phase ICGA showing a focal area of intense hyperfluorescence (hot spot; arrowhead). (Bottom) Baseline horizontal optical coherence tomography image showing cystoid macular edema and a PED. Photodynamic therapy was applied (laser spot size, 3700 μm) 1 week after IVTA.

or 2 days after IVB was injected. PDT with verteporfin was administered according to the protocol of the Treatment of Age-Related Macular Degeneration with Photodynamic Therapy study.[30] A 689-nm laser system (Carl Zeiss Meditec) was used and 50 J/cm^2 energy was delivered with an 83-second exposure time. The greatest linear dimension (GLD) was measured based on FA findings. The laser spot size was determined by FA (FA-guided PDT) in 20 eyes and by ICGA (ICGA-guided PDT) in 5 eyes. FA-guided PDT was performed for the entire lesion seen on FA. ICGA-guided PDT was chosen if the lesion comprised a larger subretinal hemorrhage at least 1 disc diameter in size.

All patients were examined 3, 6, 9, and 12 months after the initial PDT was administered. Statistical analysis was performed using the Student *t* test to compare the VA and the central retinal thickness 3, 6, 9, and 12 months from baseline.

RESULTS

TABLES 1 AND 2 SHOW THE CHARACTERISTICS AND CLINICAL data of the 22 patients (25 eyes) at baseline and after treatment. All patients were Japanese and were observed

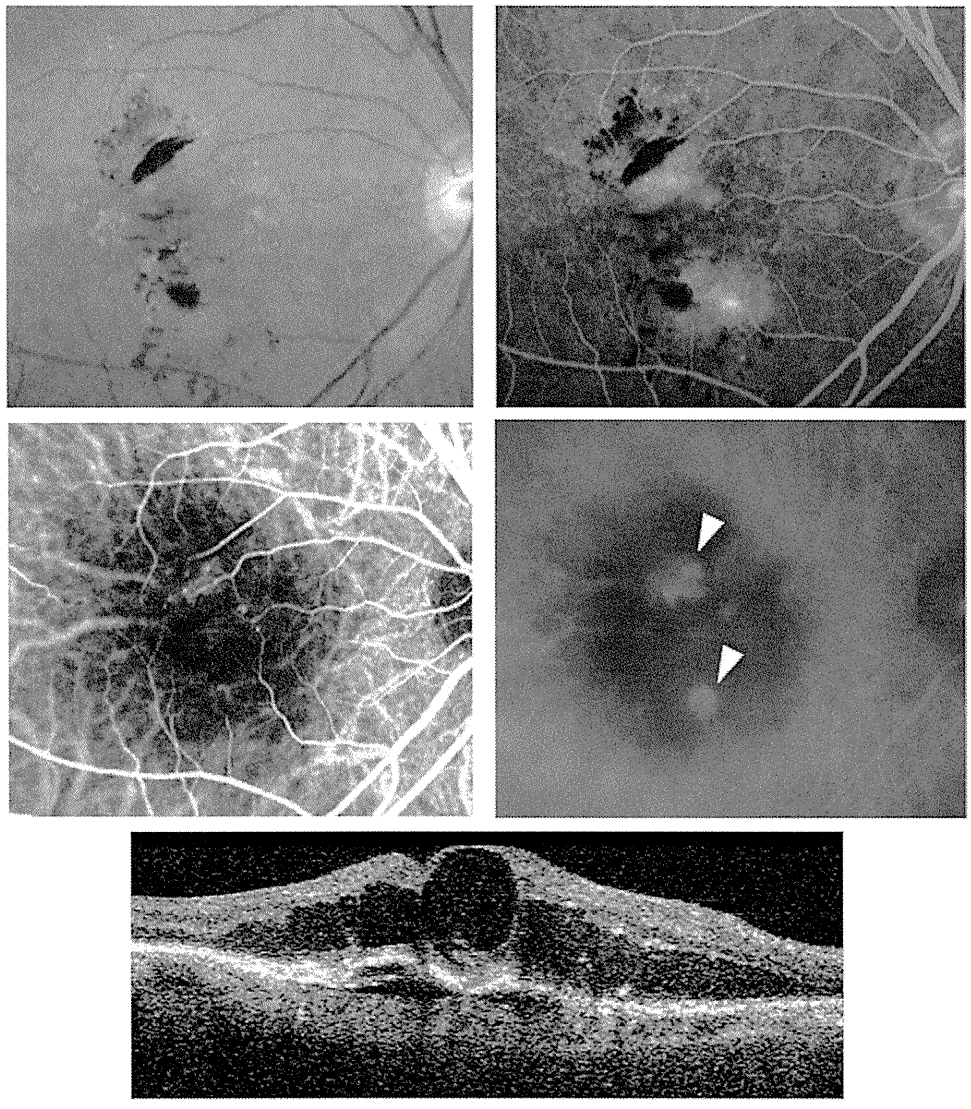

FIGURE 4. Case 7: 12 months after combined intravitreal triamcinolone acetonide with photodynamic therapy (IVTA plus PDT). Four treatments with combined therapy of IVTA plus PDT were administered over 12 months. The best-corrected visual acuity (VA) declined from 0.6 to 0.08 decimal VA. (Top left and right) Fluorescein angiograms showing that a hemorrhage, a shallow pigment epithelial detachment (PED), and leakage remain. (Middle left and right) Indocyanine green angiogram showing persistent and new retinal-retinal anastomosis and hot spots (arrowheads). (Bottom) Horizontal optical coherence tomography image showing persistent cystoid macular edema and a PED. A fifth treatment was administered.

for 12 months. There was no difference in the mean age between the 2 groups. In the 12 eyes treated with IVTA plus PDT, 7 eyes had stage 2 RAP without a retinal pigment epithelial detachment (PED) and 5 eyes had stage 2 RAP with a PED. In the 13 eyes treated with IVB plus PDT, 5 eyes had stage 2 RAP without a PED, 6 eyes had stage 2 RAP with a PED, and 2 eyes had stage 3 RAP. The mean GLD of the entire lesion was 2670 μm. There was no significant difference in the baseline patient characteristics between the 2 treatment groups.

In the 12 eyes treated with IVTA plus PDT, the mean BCVA levels at baseline and 3, 6, 9, and 12 months after treatment were 0.29, 0.25, 0.27, 0.22, and 0.13, respectively (Figure 1), indicating a significant ($P < .05$, paired t test) decline in the mean BCVA from baseline at 12 months. The mean changes in the BCVA at 6 and 12 months from baseline were a decline of 0.19 and 3.28 lines, respectively. One of the 12 eyes (8.3%) had an increase in the BCVA of 3 lines or more, 10 eyes (83.4%) had stable VA, and 1 eye (8.3%) had a decrease in the BCVA of 3 lines or more 6 months from baseline. At 12 months, 2 (16.7%) of 12 eyes had an increase in the BCVA of 3 lines or more, 7 eyes (58.3%) had stable VA, and 3 eyes (25%) had a decrease in the BCVA of 3 lines or more from baseline (Figure 2). The central retinal thickness significantly ($P < .05$, paired t test) decreased from baseline from 406 ± 125 μm (mean ± standard deviation) to 287 ± 124 μm at 3 months, 274 ± 174 μm at 6 months, 261 ± 208

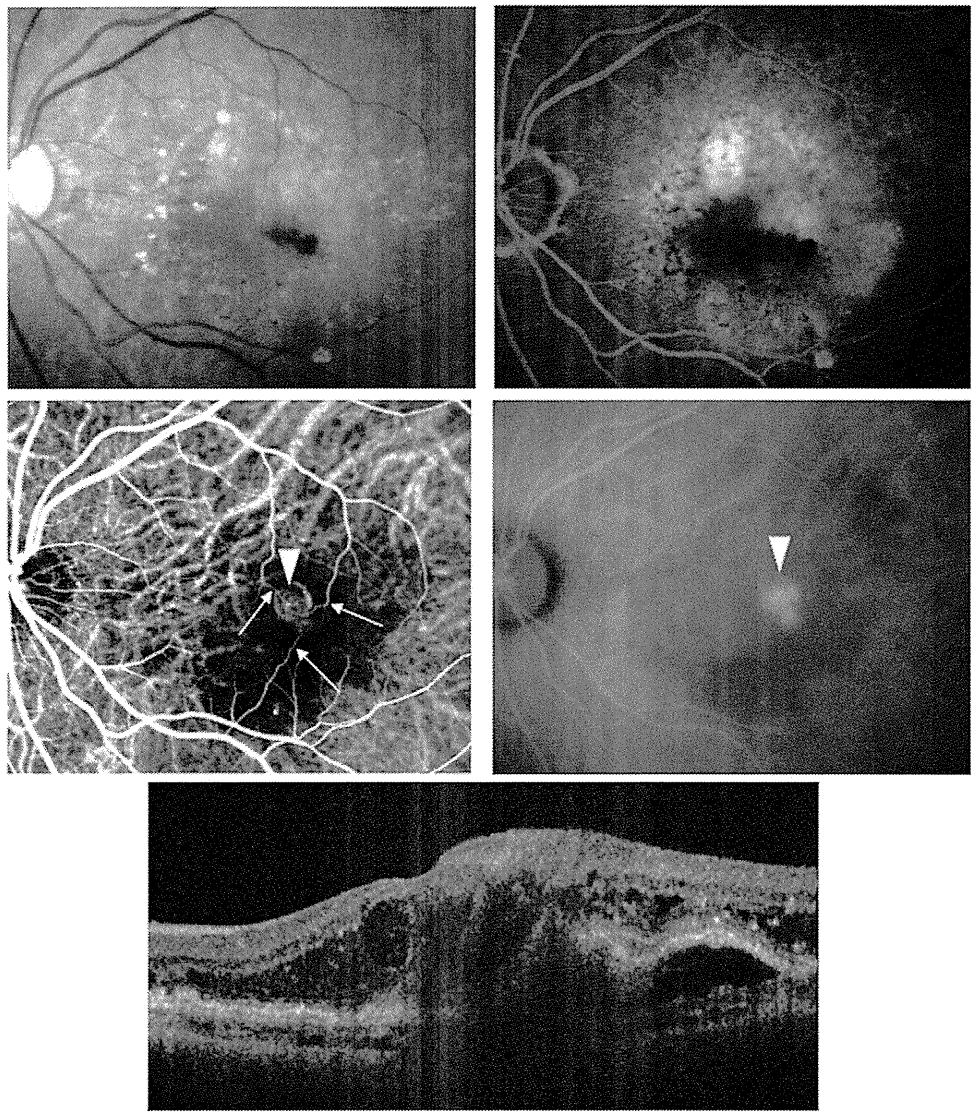

FIGURE 5. Case 22: an 83-year-old woman was treated with combined therapy of intravitreal bevacizumab and photodynamic therapy (IVB plus PDT) for stage 2 retinal angiomatous proliferation (RAP) with a pigment epithelial detachment (PED). At baseline, the best-corrected visual acuity (VA) was 0.3 decimal VA in the left eye with stage 2 RAP with a PED. (Top left) Red-free photograph showing small intraretinal and preretinal hemorrhages, a PED, and drusen. (Top right) Fluorescein angiogram showing leakage and intraretinal edema. (Middle left) Early-phase indocyanine green angiogram (ICGA) showing retinal-retinal anastomosis (arrows) and a RAP lesion (arrowhead). (Middle right) Late-phase ICGA showing a focal area of intense hyperfluorescence (hot spot; arrowhead). (Bottom) Baseline vertical optical coherence tomography image showing cystoid macular edema and a PED. Photodynamic therapy was applied (laser spot size, 5600 μm) 2 days after IVB.

μm at 9 months, and 276 ± 166 μm at 12 months. At baseline, cystoid macular edema (CME) was observed in 11 of the 12 eyes; there was a serous retinal detachment (SRD) in 7 of the 12 eyes, and a PED in 5 of the 12 eyes. The CME resolved in 5 (45.5%) eyes a mean of 5.4 weeks after baseline and decreased in 6 eyes. The SRD resolved completely in 5 (71.4%) eyes a mean of 3.1 weeks after baseline and decreased in 2 eyes. The PED resolved completely in 2 (40%) eyes a mean of 6.5 weeks after baseline and remained in 3 eyes. The mean GLD of the entire lesion was 2885 μm at baseline and 936 μm at 12 months ($P = .06$ compared with baseline). Six eyes were phakic and 6 eyes were pseudophakia. The mean intraocular pressure (IOP) was 13.7 mm Hg at baseline and 13.3 mm Hg at 12 months. Figures 3 and 4 show ocular images obtained from a patient treated with IVTA plus PDT.

In the 13 eyes treated with IVB plus PDT, the mean BCVA levels at baseline and 3, 6, 9, and 12 months after treatment were 0.25, 0.35, 0.35, 0.34, and 0.37, respectively (Figure 1). A significant improvement in the mean BCVA from baseline was seen at 3, 6, and 12 months ($P < .01$, $P < .05$, $P < .05$, respectively, paired t test; Figure 1).

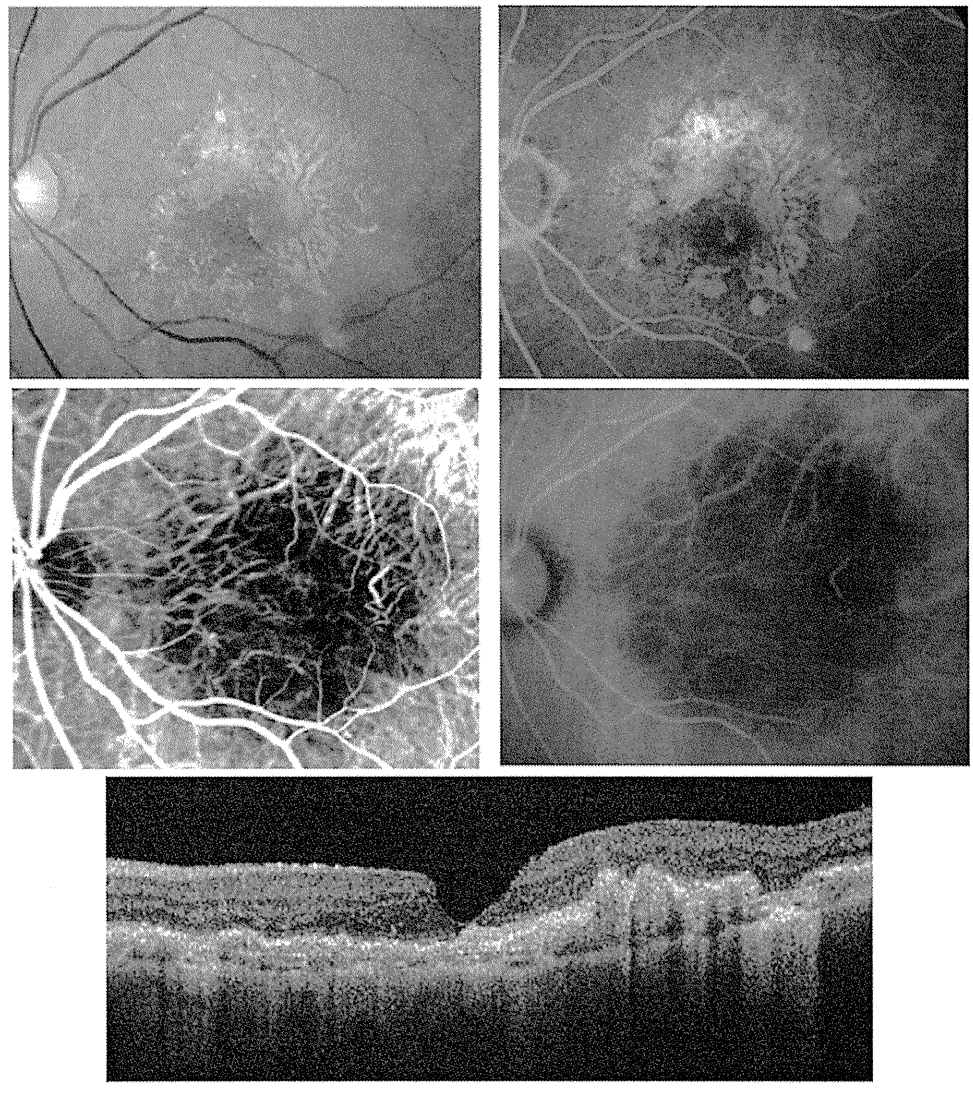

FIGURE 6. Case 22: 12 months after combined therapy of intravitreal bevacizumab and photodynamic therapy (IVB plus PDT). Three treatments were administered over 12 months. The best-corrected visual acuity (VA) improved from 0.3 to 0.6 decimal VA. (Top left and right) Fluorescein angiogram showing no hemorrhages, pigment epithelial detachment (PED), or leakage. (Middle left and right) Indocyanine green angiogram showing clear resolution of the retinal-retinal anastomosis and a hot spot. (Bottom) Vertical optical coherence tomography image showing absorption of the cystoid macular edema and a PED.

Although there was no significant difference in the mean BCVA at baseline between the 2 treatment groups ($P = .74$), there was a significant difference in the mean BCVA at 12 months ($P < .05$, nonpaired t test; Figure 1). The mean changes in BCVA at 6 and 12 months from baseline were improvements of 1.46 and 1.73 lines, respectively. The mean changes in BCVA at 3, 6, and 12 months were significantly better in the IVB plus PDT group than in the IVTA plus PDT group ($P < .05$, $P < .05$, $P < .01$, respectively, using the nonpaired t test). Four (30.8%) of the 13 eyes had an increase in the BCVA of 3 lines or more, and 9 eyes (69.2%) had stable VA at 6 months. At 12 months, 6 (46%) of 13 eyes had an increase in the BCVA of 3 lines or more, and 7 eyes (54%) had stable VA from baseline (Figure 2). No patient had decreased BCVA of 3 lines or more after treatment during any 12 months. The central retinal thickness decreased significantly from 456 ± 171 μm at baseline to 229 ± 213 μm at 3 months ($P < .01 \times 10^{-3}$), 233 ± 162 μm at 6 months ($P < .01 \times 10^{-5}$), 164 ± 120 μm at 9 months ($P < .01 \times 10^{-3}$), and 135 ± 94 μm at 12 months ($P < .01 \times 10^{-4}$). At baseline, all 13 eyes had CME, 8 of the 13 eyes had an SRD, and 8 of the 13 eyes had a PED. The CME resolved in 11 (84.6%) eyes a mean of 2.4 weeks after baseline and decreased in 2 eyes. The SRD resolved in 7 (87.5%) eyes 3.9 weeks after baseline and decreased in 1 eye. The PED resolved in 4 (50%) eyes a mean of 4.4 weeks after baseline and decreased in 3 eyes. The mean GLD of the entire lesion was 3108 μm at baseline and 0 μm at 12 months ($P < .01 \times 10^{-3}$, compared with baseline). Eight eyes

were phakic and 5 eyes were pseudophakia. The mean IOP was 14.1 mm Hg at baseline and 12.1 mm Hg at 12 months. Figures 5 and 6 show ocular images obtained from a patient treated with IVB plus PDT. The mean numbers of treatments at 12 months in the IVTA plus PDT and IVB plus PDT groups were 2.7 and 1.6, respectively, a difference that reached significance ($P < .05$, nonpaired t test). At the 12-month follow-up, FA showed resolution of leakage in all eyes treated with IVB plus PDT and resolution of leakage in 8 of the 12 eyes treated with IVTA plus PDT; the remaining 4 eyes underwent retreatments for persistent leakage.

At baseline, early-phase ICGA identified retinal–retinal anastomosis in 11 of 12 eyes treated with IVTA plus PDT and in 10 of 13 eyes treated with IVB plus PDT. Three months after treatment, complete occlusion of the retinal–retinal anastomosis was achieved in 1 (9.1%) of the 11 eyes treated with IVTA plus PDT and in 6 (60%) of the 10 eyes treated with IVB plus PDT. Among the remaining eyes (10 eyes treated with IVTA plus PDT and 4 eyes treated with IVB plus PDT) without occlusion of the retinal–retinal anastomosis, early-phase ICGA showed that the retinal–retinal anastomosis had narrowed in 1 of the 10 eyes treated with IVTA plus PDT and in all 4 eyes treated with IVB plus PDT. Moreover, 12 months after the initial treatment, complete occlusion of the retinal–retinal anastomosis was achieved in 2 (18.2%) of the 11 eyes treated with IVTA plus PDT and in 8 (80%) of the 10 eyes treated with IVB plus PDT.

Late-phase ICGA at baseline showed a hot spot in 11 of 12 eyes treated with IVTA plus PDT and in 12 of 13 eyes treated with IVB plus PDT. In 3 (27.2%) of the 11 eyes treated with IVTA plus PDT and in 100% of the 13 eyes treated with IVB plus PDT, the hot spot resolved 3 months after treatment. Moreover, 12 months after the initial treatment, the hot spot resolved in 2 (18.2%) of the 11 eyes treated with IVTA plus PDT and in 100% of the 13 eyes treated with IVB plus PDT. No complications, such as inflammation, increases in IOP to more than 21 mm Hg, severe vision loss, endophthalmitis, progression of cataract, or systemic events, developed.

DISCUSSION

THE CURRENT STUDY SHOWED THAT COMBINED TREATMENT of IVB plus PDT significantly improved the VA and reduced the number of treatments in patients with RAP compared with combined treatment of IVTA plus PDT during a 12-month follow-up.

The natural course of RAP has been reported to have poor visual outcomes compared with that of typical AMD.[5–7] The general consensus is that the disease is associated with a poor functional prognosis and resultant disciform scarring.[1,6,7] Conventional laser photocoagulation,[6,8] transpupillary thermotherapy,[6,9] surgical ablation,[10,11,30] and PDT alone[12,13] have been used to treat patients with RAP. However, poor visual outcomes usually result from these monotherapies.[6,8–13]

We reported the efficacy of IVB plus PDT for treating RAP with 6 months of follow-up.[29] In the current study, we found a significant ($P < .05$, paired t test) improvement in the mean BCVA from baseline at 12 months. The BCVA in 6 (46%) of 13 eyes increased by 3 lines or more, and 7 eyes (54%) had stable VA.

An inflammatory response and upregulation of VEGF have been reported after application of PDT.[31,32] TA has antiangiogenic, antiinflammatory, and anti-VEGF effects.[17,18] Combination therapy of PDT and TA reduced the inflammatory response and upregulation of VEGF associated with CNV and PDT. Freund and associates reported that combination therapy of IVTA plus PDT reduced or eliminated edema, achieved rapid regression of neovascularization, and stabilized or improved VA in white patients with RAP.[19] Those authors speculated that verteporfin may leak into the retinal cystic spaces, and to avoid predisposing the retinal layers to photochemical damage, they applied PDT 1 week after IVTA (referred to as pharmacology-pause-PDT). Because this method was well conceived, we administered IVTA plus PDT accordingly. Nevertheless, a significant ($P < .05$, paired t test) decline in the mean BCVA from baseline was observed at 12 months. The reason why pharmacology-pause-PDT was ineffective for treating Japanese patients in the current study is unknown.

Intraretinal neovascularization, subretinal neovascularization, and retinal–retinal anastomosis are evidence of RAP lesions.[1] Surgical lysis of the feeding arterioles and draining venules was effective because it eliminated high-flow blood supply to the RAP lesions.[33] Achieving complete occlusion of the retinal–retinal anastomosis is important for reducing RAP lesions. In patients with RAP, several injections of IVB monotherapy were needed but did not achieve complete occlusion of the feeder vessels.[34,35] We reported the efficacy of IVB plus PDT for RAP for achieving complete occlusion of retinal–retinal anastomosis during a 6-month follow-up.[29] In the current study, complete occlusion of the retinal–retinal anastomosis was achieved in 2 (18.2%) of the 11 eyes treated with IVTA plus PDT and in 8 (80%) of the 10 eyes treated with IVB plus PDT 12 months after treatment. IVB plus PDT can reduce the high-flow blood supply to RAP lesions over a long period.

Rouvas and associates compared ranibizumab, ranibizumab combined with PDT, and IVTA plus PDT with a minimum 6-month follow-up.[20] In that report, the mean VA at baseline to the end of the follow-up decreased from 0.83 to 0.85 logMAR in eyes treated with ranibizumab, decreased from 0.61 to 0.63 logMAR in eyes treated with ranibizumab plus PDT, and improved from 0.92 to 0.61 logMAR ($P = .183$) in eyes treated with IVTA plus PDT. The authors concluded that all therapies resulted in

stabilized disease, whereas IVTA plus PDT achieved better functional and anatomic results compared with the other treatments. In the current study, the mean BCVA improved significantly from 0.25 at baseline to 0.37 at 12 months in eyes treated with IVB plus PDT ($P < .05$). The investigators suggested that bevacizumab has a longer half-life than ranibizumab, so they did not observe any differences in ranibizumab and ranibizumab in combination with PDT as when using bevacizumab.

We performed PDT 1 or 2 days after administering IVB. Overexpression of VEGF in the retina (photoreceptors) is sufficient to cause intraretinal and subretinal neovascularization in animal models,[36] which is similar to the neovascular process of RAP. Using injections of intravitreal anti-VEGF agents combined with PDT is reasonable for inhibiting VEGF-induced PDT and the neovascularization of RAP. Rouvas and associates administered PDT 7 ± 2 days after ranibizumab was injected intravitreously.[20] The ideal interval between intravitreal injection of anti-VEGF agents and PDT is unknown and remains controversial. Freund and associates reported that 1 intravitreal ranibizumab injection to treat RAP resulted in rapid resolution of the intraretinal edema, hemorrhage, and neovascular lesions.[2] In typical AMD eyes, the central retinal thickness measurements decreased immediately after injection of ranibizumab.[37,38] The clinical efficacy may depend on the suppression of CNV using anti-VEGF agents. Verteporfin may accumulate minimally in the suppressed neovascular complex after injection of intravitreal anti-VEGF agents. For this reason, we applied PDT as soon as possible after IVB. Applying PDT simultaneously with intravitreal anti-VEGF agents also may be effective.

Development of complications after PDT, such as severe vision loss of approximately 4.5% in the first year[30] or the enlargement of the hypofluorescence on ICGA, has been reported.[39] The complications after IVTA include elevated IOP, progression of cataracts in phakic patients, and development of endophthalmitis.[40,41] In the current study, no patients had severe vision loss, IOP of more than 21 mm Hg, or cataract progression during the 12 months of follow-up.

In conclusion, the results of the current study indicate that combined therapy of IVB plus PDT was significantly more effective for maintaining or improving VA and reducing the number of treatments in patients with RAP compared with combined therapy of IVTA and PDT. Because this was a pilot study, larger and long-term prospective randomized studies are needed to determine the efficacy and safety profiles of combined bevacizumab or of an anti-VEGF agent and PDT.

THE AUTHORS INDICATE NO FINANCIAL SUPPORT OR FINANCIAL CONFLICT OF INTEREST. INVOLVED IN DESIGN AND conduct of study (M.S., T.I., F.S.); Collection, management, analysis, and interpretation of the data (M.S., C.S., M.K.); preparation, review, and revision of the manuscript (M.S., T.I.); and Approval of the manuscript (M.S., C.S., F.S., M.K., T.I.). The treatments in this study were approved by the Institutional Review Board/Ethics Committee of Fukushima Medical University and Kagawa University in Japan. After the potential risks and benefits were explained in detail, all patients provided written informed consent.

REFERENCES

1. Yannuzzi LA, Negrão S, Iida T, et al. Retinal angiomatous proliferation in age-related macular degeneration. Retina 2001;21:416–434.
2. Freund KB, Ho IV, Barbazetto IA, et al. Type 3 neovascularization: the expanded spectrum of retinal angiomatous proliferation. Retina 2008;28:201–211.
3. Cohen SY, Creuzot-Garcher C, Darmon J, et al. Types of choroidal neovascularisation in newly diagnosed exudative age-related macular degeneration. Br J Ophthalmol 2007;91:1173–1176.
4. Maruko I, Iida T, Saito M, Nagayama D, Saito K. Clinical characteristics of exudative age-related macular degeneration in Japanese patients. Am J Ophthalmol 2007;144:15–22.
5. Hartnett ME, Weiter JJ, Staurenghi G, Elsner AE. Deep retinal vascular anomalous complexes in advanced age-related macular degeneration. Ophthalmology 1996;103:2042–2053.
6. Bottoni F, Massacesi A, Cigada M, Viola F, Masicco I, Staurenghi G. Treatment of retinal angiomatous proliferation in age-related macular degeneration: a series of 104 cases of retinal angiomatous proliferation. Arch Ophthalmol 2005;123:1644–1650.
7. Bressler NM. Retinal anastomosis to choroidal neovascularization: a bum rap for a difficult disease. Arch Ophthalmol 2005;123:1741–1743.
8. Slakter JS, Yannuzzi LA, Schneider U, et al. Retinal choroidal anastomoses and occult choroidal neovascularization in age-related macular degeneration. Ophthalmology 2000;107:742–753.
9. Kuroiwa S, Arai J, Gaun S, Iida T, Yoshimura N. Rapidly progressive scar formation after transpupillary thermotherapy in retinal angiomatous proliferation. Retina 2003;23:417–420.
10. Sakimoto S, Gomi F, Sakaguchi H, Tano Y. Recurrent retinal angiomatous proliferation after surgical ablation. Am J Ophthalmol 2005;139:917–918.
11. Shiragami C, Iida T, Nagayama D, Baba T, Shiraga F. Recurrence after surgical ablation for retinal angiomatous proliferation. Retina 2007;27:198–203.
12. Boscia F, Furino C, Sborgia L, Reibaldi M, Sborgia C. Photodynamic therapy for retinal angiomatous proliferations and pigment epithelium detachment. Am J Ophthalmol 2004;138:1077–1079.
13. Silva RM, Cachulo ML, Figueira J, de Abreu JR, Cunha-Vaz JG. Chorioretinal anastomosis and photodynamic therapy: a two-year follow-up study. Graefes Arch Clin Exp Ophthalmol 2007;245:1131–1139.
14. Kvanta A, Algvere PV, Berglin L, Seregard S. Subfoveal fibrovascular membranes in age-related macular degeneration express vascular endothelial growth factor. Invest Ophthalmol Vis Sci 1996;37:1929–1934.

15. Kliffen M, Sharma HS, Mooy CM, Kerkvliet S, de Jong PT. Increased expression of angiogenic growth factors in age-related maculopathy. Br J Ophthalmol 1997;81:154–162.
16. Oh H, Takagi H, Takagi C. The potential angiogenic role of macrophages in the formation of choroidal neovascular membranes. Invest Ophthalmol Vis Sci 1999;40:1891–1898.
17. Penfold PL, Wen L, Madigan MC, King NJ, Provis JM. Modulation of permeability and adhesion molecule expression by human choroidal endothelial cells. Invest Ophthalmol Vis Sci 2002;43:3125–3130.
18. Hori Y, Hu DE, Yasui K, Smither RL, Gresham GA, Fan TP. Differential effects of angiostatic steroids and dexamethasone on angiogenesis and cytokine levels in rat sponge implants. Br J Pharmacol 1996;118:1584–1591.
19. Freund KB, Klais CM, Eandi CM, et al. Sequenced combined intravitreal triamcinolone and indocyanine green angiography-guided photodynamic therapy for retinal angiomatous proliferation. Arch Ophthalmol 2006;124:487–492.
20. Rouvas AA, Papakostas TD, Vavvas D, et al. Intravitreal ranibizumab, intravitreal ranibizumab with PDT, and intravitreal triamcinolone with PDT for the treatment of retinal angiomatous proliferation: a prospective study. Retina 2009; 29:536–544.
21. Krzystolik MG, Afshari MA, Adamis AP, et al. Prevention of experimental choroidal neovascularization with intravitreal anti-vascular endothelial growth factor antibody fragment. Arch Ophthalmol 2002;120:338–346.
22. Gragoudas ES, Adamis AP, Cunningham ET Jr, Feinsod M, Guyer DR, VEGF Inhibition Study in Ocular Neovascularization Clinical Trial Group. Pegaptanib for neovascular age-related macular degeneration. N Engl J Med 2004;351: 2805–2816.
23. Spaide RF, Laud K, Fine HF, et al. Intravitreal bevacizumab treatment of choroidal neovascularization secondary to age-related macular degeneration. Retina 2006;26:383–390.
24. Rosenfeld PJ, Brown DM, Heier JS, et al, MARINA Study Group. Ranibizumab for neovascular age-related macular degeneration. N Engl J Med 2006;355:1419–1431.
25. Brown DM, Kaiser PK, Michels M, et al. ANCHOR Study Group Ranibizumab versus verteporfin for neovascular age-related macular degeneration. N Engl J Med 2006;355:1432–1444.
26. Dhalla MS, Shah GK, Blinder KJ, Ryan EH Jr, Mittra RA, Tewari A. Combined photodynamic therapy with verteporfin and intravitreal bevacizumab for choroidal neovascularization in age-related macular degeneration. Retina 2006;26:988–993.
27. Ladas ID, Kotsolis AI, Papakostas TD, Rouvas AA, Karagiannis DA, Vergados I. Intravitreal bevacizumab combined with photodynamic therapy for the treatment of occult choroidal neovascularization associated with serous pigment epithelium detachment in age-related macular degeneration. Retina 2007;27:891–896.
28. Kaiser PK, Registry of Visudyne AMD Therapy Writing Committee, Boyer DS, Garcia R, et al. Verteporfin photodynamic therapy combined with intravitreal bevacizumab for neovascular age-related macular degeneration. Ophthalmology 2009;116:747–755.
29. Saito M, Shiragami C, Shiraga F, Nagayama D, Iida T. Combined intravitreal bevacizumab and photodynamic therapy for retinal angiomatous proliferation. Am J Ophthalmol 2008;146:935–941.
30. Treatment of Age-Related Macular Degeneration with Photodynamic Therapy (TAP) Study Group. Photodynamic therapy of subfoveal choroidal neovascularization in age-related macular degeneration with verteporfin: one-year results of 2 randomized clinical trials—TAP Report 1. Arch Ophthalmol 1999;117:1329–1345.
31. Tatar O, Adam A, Shinoda K, et al. Influence of verteporfin photodynamic therapy on inflammation in human choroidal neovascular membranes secondary to age-related macular degeneration. Retina 2007;27:713–723.
32. Tatar O, Adam A, Shinoda K, et al. Expression of VEGF and PEDF in choroidal neovascular membranes following verteporfin photodynamic therapy. Am J Ophthalmol 2006;142: 95–104.
33. Borrillo JL, Sivalingam A, Martidis A, Federman JL. Surgical ablation of retinal angiomatous proliferation. Arch Ophthalmol 2003;121:558–561.
34. Meyerle CB, Freund KB, Iturralde D, et al. Intravitreal bevacizumab (Avastin) for retinal angiomatous proliferation. Retina 2007;27:451–457.
35. Joeres S, Heussen FM, Treziak T, Bopp S, Joussen AM. Bevacizumab (Avastin) treatment in patients with retinal angiomatous proliferation. Graefes Arch Clin Exp Ophthalmol 2007;245:1597–1602.
36. Okamoto N, Tobe T, Hackett SF, et al. Transgenic mice with increased expression of vascular endothelial growth factor in the retina: a new model of intraretinal and subretinal neovascularization. Am J Pathol 1997;151:281–291.
37. Fung AE, Lalwani GA, Rosenfeld PJ, et al. An optical coherence tomography-guided, variable dosing regimen with intravitreal ranibizumab (Lucentis) for neovascular age-related macular degeneration. Am J Ophthalmol 2007;143: 566–583.
38. Kiss CG, Geitzenauer W, Simader C, et al. Evaluation of ranibizumab-induced changes in high-resolution optical coherence tomographic retinal morphology and their impact on visual function. Invest Ophthalmol Vis Sci 2009;50: 2376–2383.
39. Rouvas AA, Papakostas TD, Ladas ID, Vergados I. Enlargement of the hypofluorescent post photodynamic therapy treatment spot after a combination of photodynamic therapy with an intravitreal injection of bevacizumab for retinal angiomatous proliferation. Graefes Arch Clin Exp Ophthalmol 2008;246:315–318.
40. Spaide RF, Sorenson J, Maranan L. Combined photodynamic therapy with verteporfin and intravitreal triamcinolone acetonide for choroidal neovascularization. Ophthalmology 2003; 110:1517–1525.
41. Bhavsar AR, Ip MS, Glassman AR, DRCRnet and the SCORE Study Groups. The risk of endophthalmitis following intravitreal triamcinolone injection in the DRCRnet and SCORE clinical trials. Am J Ophthalmol 2007;144:454–456.

Morphologic Changes in the Outer Layer of the Detached Retina in Rhegmatogenous Retinal Detachment and Central Serous Chorioretinopathy

ICHIRO MARUKO, TOMOHIRO IIDA, TETSUJU SEKIRYU, AND MASAAKI SAITO

• PURPOSE: To examine changes in the outer layer of the detached retina in rhegmatogenous retinal detachment (RRD) and central serous chorioretinopathy (CSC) with optical coherence tomography (OCT).

• DESIGN: Retrospective, observational case series.

• METHODS: Fifteen eyes (15 patients) with RRD and 16 eyes (16 patients) with acute CSC were studied by OCT-ophthalmoscope. All patients had a macular detachment within 1 month after subjective onset. We measured the height of the foveal RD and the thicknesses of the outer nuclear layer (ONL) and the detached neurosensory retina; the thickness of the latter two were measured at the thickest points within 2 degrees of the center of the fovea using vertical and horizontal scans at the initial OCT examination.

• RESULTS: The mean best-corrected visual acuity (BCVA) after reattachment improved in both groups. The ONL was significantly thicker in the RRD group than in the CSC group (133.7 ± 62 μm, 67.0 ± 12.0 μm; $P < .001$). There was no significant difference in the thickness of the detached sensory retina between the groups ($P = .06$). In the RRD group, the BCVA after reattachment was correlated with the thickness of the ONL and the height of the detachment ($R = 0.55$, $P = .03$; $R = 0.75$, $P = .004$). There were no correlations between the retinal morphologic changes and the BCVA in the CSC group.

• CONCLUSION: The ONL became thicker in patients with a RRD, and the structure of the detached sensory retina was preserved in patients with CSC. The difference in the morphologic changes in the ONL in RD might be associated with visual function. (Am J Ophthalmol 2009; 147:489–494. © 2009 by Elsevier Inc. All rights reserved.)

ALTHOUGH BOTH RHEGMATOGENOUS RETINAL DETACHMENT (RRD) and central serous chorioretinopathy (CSC) are associated with macular detachment, their visual outcomes and prognoses differ. Optical coherence tomography (OCT) is a noninvasive imaging technique that can help diagnose and predict visual outcomes. Using OCT, several groups have reported the morphologic changes in the detached retina in RRD and acute CSC using OCT.[1–6]

In RRD with a macular detachment, the height of the RD and the intraretinal separation are associated with poor visual function after resolution.[1–3] In CSC with macular detachment, thickening, granulation, and atrophy of the neurosensory retinal layer contribute to visual loss after reattachment.[4–6]

The OCT-ophthalmoscope (OCT-C7; Nidek-OTI, Gamagori, Japan) is a device that provides confocal scanning laser ophthalmoscope (SLO) images, high-resolution cross-sectional (longitudinal) OCT images, and coronal (transversal) OCT images at different depths through the posterior fundus.[7–15] The SLO images and the OCT images correspond pixel to pixel with each other, so the OCT findings can be determined accurately on the en face fundus image. Transversal (x-y axis) resolutions are about 15 μm to 20 μm and depth (z-axis) resolutions are within 10 μm. Internal software also can accurately measure the thickness and distance from the OCT images.

In the current study, we observed the structure of the detached retina in RRD and acute CSC using the OCT-ophthalmoscope.

METHODS

OF 83 EYES (82 PATIENTS) WITH RRD AND 50 EYES (50 patients) with CSC that were newly diagnosed between January 1, 2005 and December 31, 2005, 16 eyes (16 patients) with RRD and 15 eyes (15 patients) with acute CSC included the macular detachment within 1 month after subjective onset and observed by OCT-ophthalmoscope at the initial examination were studied. In the RRD group, we also excluded the patients in whom the height of the RD exceeded that measurable using OCT-C7. There were no such patients in the CSC group. Patients with other causes of RD such as age-related macular degeneration, Harada disease, posterior scleritis, and any other diseases were excluded. The average patient ages with RRD and CSC were 50 years (range, 18 to 82 years) and 43 years (range, 31 to 55 years), respectively. The follow-up periods were 8.9 ± 5.7 months (range, 2 to 26 months) in the patients with RRD and 10.5 ± 6.7 months (range, 3 to 24 months) in the patients with CSC. We measured the height of the RD at the center of the fovea and the thickness of the retinal outer nuclear layer

Accepted for publication Sep 24, 2008.

From the Department of Ophthalmology, Fukushima Medical University School of Medicine, Fukushima, Japan.

Inquiries to Ichiro Maruko, Department of Ophthalmology, Fukushima Medical University School of Medicine, 1 Hikarigaoka, Fukushima, Japan; e-mail: imaruko@fmu.ac.jp

0002-9394/09/$36.00
doi:10.1016/j.ajo.2008.09.030

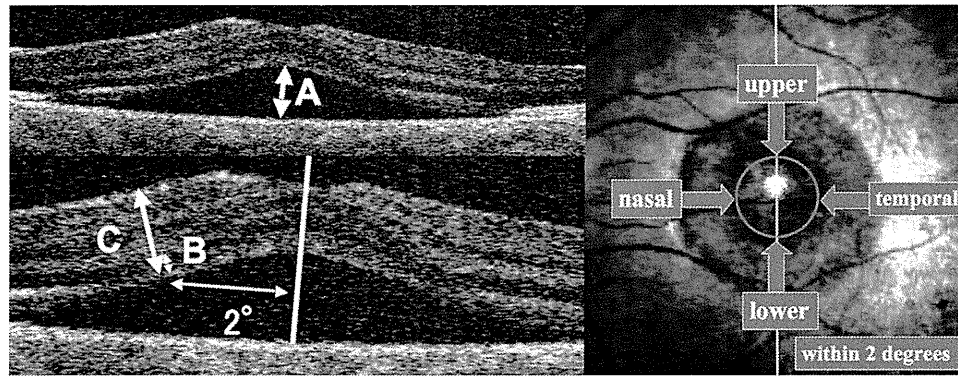

FIGURE 1. Measurement points using optical coherence tomography (OCT)-ophthalmoscopy. (Top left) The height of the retinal detachment (RD) at the center of the fovea (arrow A). (Bottom left) The thickness of the outer retinal nuclear layer (ONL) (arrow B) and the detached sensory retina (arrow C). (Right) The average thickness of the ONL and the detached sensory layer at the four points (upper, lower, nasal, and temporal) within 2 degrees is indicated.

TABLE 1. Patients' Preoperative and Postoperative Data in Rhegmatogenous Retinal Detachment Group

Patient No.	Age	Gender	BCVA Preoperative (logMAR)	BCVA Postoperative (logMAR)	Onset (days)	No. of Quadrants with Retinal Detachment	Location of Retinal Breaks	H-RD (μm)	T-ONL (μm)	T-DR (μm)	Duration (mos)	F/U (mos)
1	21	M	0.30	−0.18	1	2	superior-temporal	136	75	260	10	12
2	47	F	0.00	0.00	7	1	superior-temporal	135	85	312	9	26
3	61	F	0.22	−0.08	3	1	superior	57	90	269	1	4
4	66	M	0.15	0.15	3	1	temporal	105	97	302	2	6
5	56	F	0.15	−0.08	20	3	superior	135	99	290	3	3
6	50	F	0.22	0.00	14	2	superior-nasal	399	99	316	1	2
7	18	F	0.30	0.22	30	3	superior-inferior	917	104	325	3	7
8	46	M	0.40	−0.18	7	2	superior	105	128	328	7	7
9	18	M	0.52	0.30	26	2	superior-temporal	1329	135	302	5	11
10	47	M	0.30	0.40	7	2	superior-temporal	719	178	420	1	6
11	25	M	0.15	−0.08	3	2	temporal	456	153	421	2	10
12	74	M	2.00	0.40	7	2	superior-temporal	737	217	551	2	6
13	57	M	1.52	0.70	7	2	superior	1509	261	739	1	13
14	62	M	0.52	0.15	30	2	temporal	526	252	554	1	11
15	63	F	0.40	0.10	14	4	temporal	96	84	250	2	12
16	82	M	0.70	0.15	14	2	superior-inferior	539	83	281	1	6
Mean	50		0.49	0.12	12.1	2.1		493.8	133.7	369.8	3.2	8.9
SD	20.0				9.7			452	62	136	3.0	5.7

BCVA = best-corrected visual acuity; F = female; F/U = follow-up periods; H-RD = height of retinal detachment; logMAR = logarithm of the minimum angle of resolution; M = male; Mos = months; SD = standard deviation; T-DR = thickness of the detached retina; T-ONL = thickness of the outer nuclear layer.

(ONL) and the detached neurosensory retina. The thickness of the ONL and the detached sensory retina were measured and averaged at the four thickest points (upper, lower, nasal, and temporal) within 2 degrees of the center of the fovea using vertical and horizontal scans at the initial OCT examination (Figure 1). We defined the height of RD as the length between the outer retinal surface and the retinal pigment epithelium (RPE) at the center of the fovea, the ONL as the outer hyporeflective layer just above the outer retinal surface, and the detached neurosensory retina as the length between the inner and the outer retinal surface. The OCT-C7, which is the current device of OCT-ophthalmoscope, covers an area of 7.2 mm × 7.2 mm (equal to 24 degrees × 24 degrees) in x-y axis and 1,500 μm of depth in z-axis. Internal caliper software can accurately measure the thickness and distance from the OCT images with depth (z-axis) resolution to less than 10 μm.

We also measured the visual outcome during the follow-up period. All best-corrected visual acuity (BCVA) levels were measured with a Japanese standard decimal visual chart. As to

TABLE 2. Patients' Preoperative and Postoperative Data in Central Serous Chorioretinopathy Group

Patient No.	Age	Gender	BCVA Preoperative (logMAR)	BCVA Postoperative (logMAR)	Onset (days)	Extent (DA)	H-RD (μm)	T-ONL (μm)	T-DR (μm)	Duration (mos)	F/U (mos)
1	51	M	0.05	0.05	14	15.6	53	52	208	2	24
2	52	F	0.00	−0.18	21	4.7	329	51	244	2	12
3	49	M	1.00	−0.08	14	12.1	832	48	257	3	8
4	44	M	−0.18	−0.18	10	15.2	311	66	279	6	8
5	41	M	0.05	−0.08	3	3.9	649	84	283	6	12
6	45	F	−0.08	−0.08	21	1.1	211	89	301	3	14
7	31	F	−0.08	−0.18	21	4.8	325	64	313	2	15
8	45	M	−0.08	−0.18	5	1.9	180	64	317	3	6
9	31	M	−0.08	−0.08	21	5.7	175	61	318	1	3
10	55	M	0.10	0.00	7	6.3	325	63	325	3	3
11	52	M	0.05	−0.18	5	2.6	140	64	339	1	24
12	33	M	−0.08	−0.18	7	4.6	140	73	315	1	7
13	38	M	0.05	0.00	7	6.7	316	78	326	1	3
14	36	M	−0.08	−0.08	1	4.5	307	69	294	3	12
15	44	M	0.70	0.22	14	2.3	158	80	350	2	6
Mean	43		0.09	−0.08	11	6.1	296.7	67.0	297.8	3	10.5
SD	8.0				7.1	4.6	203	12	38	1.6	6.7

BCVA = best-corrected visual acuity; DA = disc area; F = female; F/U = follow-up periods; H-RD = height of retinal detachment; logMAR = logarithm of the minimum angle of resolution; M = male; Mos = months; SD = standard deviation; T-DR = thickness of the detached retina; T-ONL = thickness of the outer nuclear layer.

the limitations of this study, instead of measuring the BCVA by Early Treatment Diabetic Retinopathy Study (ETDRS) chart, we measured it by Japanese standard decimal visual chart. However, Japanese standard decimal visual chart values were calculated by logarithm of the minimum angle of resolution (logMAR) scale for comparing the mean BCVA. Resolution of RD was evaluated by indirect ophthalmoscopy, slit-lamp biomicroscopy with a noncontact lens, and OCT during the follow-up period. We did a comparative study of the anatomic data and the BCVA. The results were analyzed using the Student *t* test and Spearman rank correlation (R).

RESULTS

THE PATIENTS' DATA IN THE RRD AND CSC GROUPS ARE provided in Tables 1 and 2. The mean BCVA levels at baseline were, respectively, 0.32 (0.49 logMAR) in the RRD group and 0.82 (0.09 logMAR) in the CSC group. The mean BCVA levels after reattachment at the final examination were, respectively, 0.75 (0.12 logMAR) in the RRD group and 1.2 (-0.08 logMAR) in the CSC group.

The mean extent of RD area in the RRD group was about a half of total retinal area including the macular area. The postoperative BCVA was not significantly correlated in the extent of preoperative RD. The mean extent of serous RD area in the CSC group was 6.1 ± 4.6 DA (disc area), which was defined as the Macular Photocoagulation Study Disc Area (MPSDA). One MPSDA was calculated as 2.54 mm^2 based on a standard disc diameter (MPSDD) of 1.8 mm.[16] The BCVA at the final examination was not significantly correlated in the extent of serous RD area at the baseline.

The mean presumed duration of macular detachment until resolution was 3.2 months in the RRD group and 2.5 months in the CSC group, respectively. There was no significant difference.

The height of the RD at the center of the fovea was 493.8 ± 452 μm in the RRD group and 296.7 ± 203 μm in the CSC group. There was no significant difference ($P = .13$). Patients with higher elevation in the RRD group and in the CSC group had a worse BCVA at the baseline ($R = 0.56$, $P < .05$; $R = 0.51$, $P < .05$). The thickness of the ONL was 133.7 ± 62 μm in the RRD group and 67.0 ± 12 μm in the CSC group at the initial examination, a difference that reached significance ($P < .001$). The thickness of the detached sensory retina was 369.8 ± 136 μm in the RRD group and 297.8 ± 38 μm in the CSC group, a difference that did not reach significance ($P = .06$). In the RRD group, the BCVA after reattachment was correlated with the ONL thickness and the height of the detachment ($R = 0.55$, $P = .03$; $R = 0.75$, $P = .004$, respectively). There was no correlation between the retinal morphologic changes and the BCVA in the CSC group.

CASE REPORTS

• CASE 1: A 74-year-old man (Patient 12 in RRD group) with a history of cataract surgery about 1 year previously reported a 1-week loss of visual acuity (VA) in the left eye.

FIGURE 2. Case 1 (Patient 12 in the rhegmatogenous retinal detachment [RRD] group). The left eye of a 74-year-old man. (Top right) A fundus photograph shows a RD that includes the macular area caused by a tear in the superior temporal area. Arrow A on the vertical scan (Top left) and the horizontal scan (Bottom right) indicates the height of the RD using OCT-ophthalmoscope. Arrows B and C indicate the thickness of the ONL and detached retina. The height of the RD is 737 μm; the average thickness of the ONL is 217 μm (range, 167 to 268 μm); and the average thickness of the detached sensory retina average is 551 μm (range, 491 to 658 μm).

The BCVA at the baseline was 0.01 (2.00 logMAR). A RRD that included the macular area resulting from the tear at the superior-temporal area was observed during clinical examinations (Figure 2, Top right). OCT-ophthalmoscope showed a macular-off detachment at the vertical scan (Figure 2, Top left) and the horizontal scan (Figure 2, Bottom right). The height of the RD, the average thickness of the ONL, and the average thickness of the detached sensory retina measured by OCT-ophthalmoscope were 737 μm, 217 μm (range, 167 to 268 μm), and 551 μm (range, 491 to 658 μm), respectively. The patient underwent a pars plana vitrectomy with gas tamponade using 20% SF_6. Eight weeks after surgery, the retina was reattached with OCT-ophthalmoscope. The BCVA at the reattachment was 0.4 (0.40 logMAR).

• CASE 2: A 38-year-old man (Patient 13 in CSC group) complained of micropsia in his right eye of 1-week duration. The BCVA at the baseline was 0.9 (0.10 logMAR). There was no history of corticosteroid treatment. A round RD at the center of the macular area was observed during clinical examinations (Figure 3, Top left). Early-phase fluorescein angiography in the right eye showed focal leakage in the lower temporal macular area (Figure 3, Top right) and hyperfluorescence attributable to pooling in the subretinal space including the macular area in the late phase. OCT-ophthalmoscope showed the macular detachment at the horizontal scan (Figure 3, Bottom left) and the vertical scan (Figure 3, Bottom right). The height of the RD, the average ONL thickness, and the detached sensory retina measured by OCT-ophthalmoscope were 316 μm, 78 μm (range, 70 to 88 μm), and 326 μm (range, 298 to 357 μm), respectively. The macular detachment resolved without treatment 1 month later. The BCVA at the reattachment was 1.0 (0.0 logMAR).

DISCUSSION

THE ONL THICKENED IN THE RRD GROUP, AND THE STRUCTURE of the detached sensory retina was preserved in the

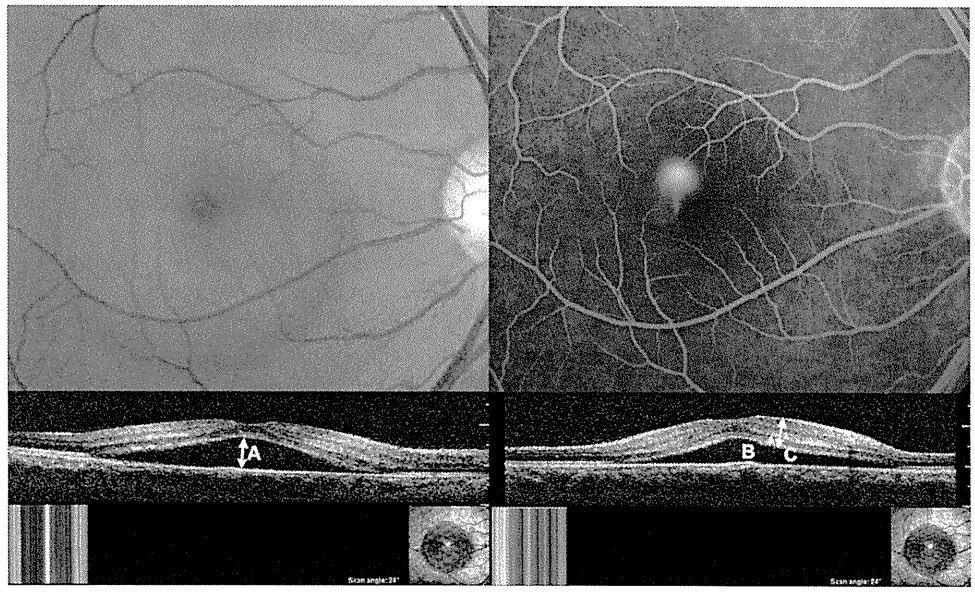

FIGURE 3. Case 2 (Patient 13 in the central serous chorioretinopathy group). The right eye of a 38-year-old man. (Top left) A fundus photograph shows a serous RD of 2 disc diameters including the macular area. (Top right) Early-phase fluorescein angiography shows fluorescence leakage from the lower temporal macular area. A horizontal scan (Bottom left) and the vertical scan (Bottom right) show a foveal RD using OCT-ophthalmoscope. Arrow A indicates the height of the RD. Arrows B and C show the ONL and the thickness of the detached retina. The height of the RD is 316 μm; the average thickness of the ONL is 78 μm (range, 70 to 88 μm); and the average thickness of the detached sensory retina is 326 μm (range, 298 to 357 μm).

CSC group. Nevertheless, both groups had acute macular detachments. The morphologic changes in the detached retina in the CSC group were not correlated with the visual outcome at the resolution of the detachment. However, the height of the detachment and the ONL thickness at the initial examination in the RRD group were correlated with the visual outcome after reattachment. Although we excluded patients in the RRD group when the height of the RD was not measurable using our OCT device, there were substantial differences between CSC and RRD in the visual outcomes and the formation of a detachment, which may indicate that the formation mechanism itself induces the differences in the visual function between the two pathologies.

A detached retina is not only mechanically stressed, but also exposed to the vitreous fluid pooled at the subretinal space through the retinal tear from the vitreous cavity in RRD. Vitreous fluid accumulated at the subretinal space breaks the outer blood-retinal barrier that forms on RPE and allows RPE cells to enter the vitreous cavity (ie, tobacco dust).[17] In the experimental models of RD, a decrease in the number of photoreceptor cells occurred within a few days.[18,19] In the experimental RD produced by injection of vitreous, inter-nuclear enlargement and proliferation of glial cells including the Müller cells were histopahthologically observed following to the disruption and disappearance of the outer segments in the photoreceptors.[20,21] These results may indicate the thickening of ONL in RRD. These subretinal fluids (SRF) and direct stress to retina may produce the swelling of the detached neurosensory retina and ONL in eyes with RRD.

Although the heights of the RD at the center of the fovea in both groups were not significantly different, the total area of RD in the RRD group was larger than in the CSC group. This might indicate there was much difference in material composition of the SRF between both groups. Poor nutrition collected from RPE and choroids in the RRD group might cause the thickness to the detached neurosensory retina and ONL.

Some studies have reported that high concentrations of glucose or oxygen supplementation prevents death of the photoreceptor cells.[22,23] The SRF in CSC is comprised of exudates from the choroid through a barrier defect in the RPE and is concentrated in a closed space compared with the fluid in RRD. Although high concentrations of fluid are thought to damage the detached retina and RPE over a long period, the retinal structure may be preserved in the short-term.

Because of the availability of OCT devices, RRD and CSC with macular detachments can be studied and understood. However, morphologic and functional study might be needed using other devices to clarify the differences in visual outcomes.

In conclusion, the ONL becomes thickened in eyes with RRD, and the structure of the detached sensory retina is preserved in eyes with CSC. The difference in the morphologic changes in the ONL associated with a RD might be associated with visual function. The patients with a thicker ONL may have worse visual outcome.

THE AUTHORS INDICATE NO FINANCIAL SUPPORT OR FINANCIAL CONFLICT OF INTEREST. INVOLVED IN DESIGN AND conduct of study (I.M., T.I.); collection (I.M., T.I., T.S., M.S.); management, analysis, and interpretation of data (I.M., T.I., T.S., M.S.); and preparation, review, and approval of the manuscript (I.M., T.I.). The Institutional Review Board (IRB) at Fukushima Medical University School of Medicine declared that this type of retrospective study waived the need for IRB approval.

REFERENCES

1. Hagimura N, Suto K, Iida T, Kishi S. Optical coherence tomography of the neurosensory retina in rhegmatogenous retinal detachment. Am J Ophthalmol 2000;129:186–190.
2. Yetik H, Guzel H, Ozkan S. Structural features of attached retina in rhegmatogenous retinal detachments. Retina 2004; 24:63–68.
3. Lecleire-Collet A, Muraine M, Menard JF, Brasseur G. Predictive visual outcome after macula-off retinal detachment surgery using optical coherence tomography. Retina 2005;25:44–53.
4. Iida T, Hagimura N, Sato T, Kishi S. Evaluation of central serous chorioretinopathy with optical coherence tomography. Am J Ophthalmol 2000;129:16–20.
5. Piccolino FC, De La Longrais RR, Ravera G, et al. The foveal photoreceptor layer and visual acuity loss in central serous chorioretinopathy. Am J Ophthalmol 2005;139:87–99.
6. Furuta M, Iida T, Kishi S. Foveal thickness can predict visual outcome in patients with persistent central serous chorioretinopathy. Ophthalmologica 2008;223:28–31.
7. Van Velthoven ME, Verbraak FD, Yannuzzi LA, Rosen RB, Podoleanu AG, de Smet MD. Imaging the retina by en face optical coherence tomography. Retina 2006;26:129–136.
8. Podoleanu AG, Dobre GM, Cucu RC, et al. Combined multiplanar optical coherence tomography and confocal scanning ophthalmoscopy. J Biomed Opt 2004;9:86–93.
9. Ikuno Y, Gomi F, Tano Y. Potent retinal anterior traction as a possible cause of myopic foveoschisis. Am J Ophthalmol 2005;139:462–467.
10. Van Velthoven ME, Verbraak FD, Garcia PM, et al. Evaluation of central serous retinopathy with en face optical coherence tomography. Br J Ophthalmol 2005;89:1483–1488.
11. Van Velthoven ME, Verbraak FD, Yannuzzi LA, et al. Imaging the retina by en face optical coherence tomography. Retina 2006;26:129–136.
12. Mitarai K, Gomi F, Tano Y. Three-dimensional optical coherence tomographic findings in central serous chorioretinopathy. Graefes Arch Clin Exp Ophthalmol 2006;244: 1415–1420.
13. Koizumi H, Iida T, Maruko I. Morphologic features of group 2A idiopathic juxtafoveolar retinal telangiectasis in three-dimensional optical coherence tomography. Am J Ophthalmol 2006;142:340–343.
14. Saito M, Iida T, Nagayama D. Cross-sectional and en face optical coherence tomographic features of polypoidal choroidal vasculopathy. Retina 2008;28:459–464.
15. Kon Y, Iida T, Maruko I, Saito M. The optical coherence tomography-ophthalmoscope for examination of central serous chorioretinopathy with precipitates. Retina 2008;28: 864–869.
16. Macular Photocoagulation Study Group. Laser photocoagulation of subfoveal neovascular lesions in age-related macular degeneration. Arch Ophthalmol 1991;109:1220–1231.
17. Tsuboi S, Taki-Noie J, Emi K, Manabe R. Fluid dynamics in eyes with rhegmatogenous retinal detachments. Am J Ophthalmol 1985;99:673–676.
18. Machemer R. Experimental retinal detachment in the owl monkey. II. Histology of retina and pigment epithelium. Am J Ophthalmol 1968;66:396–410.
19. Cook B, Lewis GP, Fisher SK, Adler R. Apoptotic photoreceptor degeneration in experimental retinal detachment. Invest Ophthalmol Vis Sci 1995;36:990–996.
20. Zhu ZR, Goodnight R, Sorgente N, Blanks JC, Ogden TE, Ryan SJ. Cellular proliferation induced by subretinal injection of vitreous in the rabbit. Arch Ophthalmol 1988;106: 406–411.
21. Abe T, Yoneya A, Mori K, Hayashi N, Isono H. Reaction of the retina to injected subretinal fluids [in Japanese]. Nippon Ganka Gakkai Zasshi 1994;98:453–462.
22. Mervin K, Valter K, Maslim J, Lewis G, Fisher S, Stone J. Limiting photoreceptor death and deconstruction during experimental retinal detachment: the value of oxygen supplementation. Am J Ophthalmol 1999;128:155–164.
23. Sakai T, Lewis GP, Linberg KA, Fisher SK. The ability of hyperoxia to limit the effects of experimental detachment in cone-dominated retina. Invest Ophthalmol Vis Sci 2001;42: 3264–3273.

Experimental Neurology 217 (2009) 401–406

Contents lists available at ScienceDirect

Experimental Neurology

journal homepage: www.elsevier.com/locate/yexnr

Objective perimetry using functional magnetic resonance imaging in patients with visual field loss

Ayumu Furuta [a,b,*], Satoshi Nakadomari [c,d], Masaya Misaki [e], Satoru Miyauchi [e], Tomohiro Iida [b]

[a] Maeda Ophthalmic Clinic, 3-30 Nakamachi, Aizuwakamatsu, Fukushima 965-0878, Japan
[b] Department of Ophthalmology, Fukushima Medical University, 1 Hikariga-oka, Fukushima City, Fukushima 960-1295, Japan
[c] Department of Functional Training III, National Rehabilitation Center for Persons with Disabilities, 1 Namiki 4-chome, Tokorozawa City, Saitama 359-8555, Japan
[d] Department of Ophthalmology, Jikei University, School of Medicine 3-25-8, Nishi-Shimbashi, Minato-ku, Tokyo 105-8461, Japan
[e] Kobe Advanced ICT Research Center, National Institute of Information and Communications Technology, 588-2, Iwaoka, Nishi-ku, Kobe, Hyogo 651-2492, Japan

ARTICLE INFO

Article history:
Received 11 December 2008
Revised 20 February 2009
Accepted 24 March 2009
Available online 5 April 2009

Keywords:
fMRI
Objective perimetry
Occipital lobes
Visual field loss

ABSTRACT

In ophthalmic clinics, subjective perimetry is a standard examination method. However, for certain patients, objective perimetry is useful since it avoids the need for subjective judgments. The purpose of the present study is to demonstrate the feasibility of objective perimetry using functional magnetic resonance imaging (fMRI). fMRI was performed in 8 patients with visual field defects caused by cerebral lesions. The composite stimulus was either the combination of an expanding ring and a clockwise rotating wedge, or a contracting ring and a counter-clockwise rotating wedge. The largest radius was a 10° visual angle with magnifying glasses. The cycle period for the ring and wedge components differed, enabling us to distinguish the two targets within a single time series. Data were analyzed using custom software that interprets the two stimuli and estimates visual field maps. Regions of interest (ROIs) were set covering the entirety of the occipital lobes, and the most effective visual field location for each voxel was calculated from these two response components. The visual field maps obtained with fMRI were compared with the 10-2 Humphrey visual field (HVF) program. While some divergences were observed, in most subjects the visual field defects on fMRI agreed with those on HVF. Cross-correlation coefficients between grayscale values of visual field maps obtained with fMRI and decibel values obtained with HVF were significant ($P<0.05$) in all subjects. fMRI in conjunction with our method is feasible for objectively and efficiently measuring the visual field of patients with visual field loss.

Introduction

Functional magnetic resonance imaging (fMRI) has recently been used to investigate visual brain function. This method allows non-invasive measurement of the representation of the visual field in the human occipital cortex (Engel et al., 1994, 1997; Sereno et al., 1994; Tootell et al., 1996; Wandell et al., 2000; Wandell and Wade, 2003). fMRI has also been applied to research for patients with visual field defects (Duncan et al., 2007; Kollias et al., 1998; Lee et al., 2001; Wong and Sharpe, 1999).

In ophthalmic clinics, while subjective perimetry is a standard examination method, objective perimetry is useful for certain patients since it avoids the need for subjective judgments. Objective perimetry has been studied using various methods including pupil response (Kardon et al., 1991), electroretinography (Bearse and Sutter, 1996), visual evoked potential (Baseler et al., 1994; Kim et al., 2006; Klistorner et al., 2005; Yukawa et al., 2008), and magnetoencephalography (Nishiyama et al., 2004). In principle, fMRI can be used as a method of objective perimetry. In ophthalmic practice, subjective perimetry findings often differ from other clinical findings, making it difficult to make a diagnosis. For example, a subjective perimetry finding suggesting a significant constricting scotoma with the lack of an apparent lesion that supports the subjective finding may result in a diagnosis of psychogenic visual disturbance. In such cases, the physician cannot be completely sure of the diagnosis since the presence of an organic disorder still cannot be ruled out. A similar difficulty in diagnosis is encountered when dealing with patients suspected of malingering. In patients with left unilateral spatial neglect due to right parietal damage, it is important to confirm the presence or absence of left homonymous hemianopsia when undertaking rehabilitation. It is, however, difficult to distinguish between neglect and hemianopsia based on subjective perimetry or clinical symptoms. In these cases, it would be clinically very useful to undertake objective perimetry using fMRI since it may be able to prove that a visual field considered to be lost by a subjective test is in fact intact. However, there are difficulties in applying fMRI perimetry in clinics. For example, fMRI experiments take a long time, and data analysis is not easy. Our goal is to simplify the fMRI perimetry method to make it practical for use in clinics. We previously arranged visual

* Corresponding author. Maeda Ophthalmic Clinic, 3-30 Nakamachi, Aizuwakamatsu, Fukushima 965-0878, Japan. Fax: +81 242 29 3556.
E-mail address: ayumu@mxy.mesh.ne.jp (A. Furuta).

0014-4886/$ – see front matter © 2009 Elsevier Inc. All rights reserved.
doi:10.1016/j.expneurol.2009.03.030

Table 1
Profile of subjects.

Subject	Age (Y)	Sex	BCVA (R, L)	Cause	Lesions on MRI	Time post-lesion
1	23	Male	(1.2, 1.2)	Traumatic CC	L. temporal lobe, R. parietal lobe	8M
2	67	Male	(1.0, 1.0)	Cardiogenic CI (R. PCA infarction)	R. occipital lobe	7Y
3	37	Male	(1.2, 1.2)	Traumatic CC	R. occipital lobe, R. temporal lobe	20Y
4	57	Male	(1.2, 1.2)	Hypoxemia associated with laryngeal spasm	Global cerebral atrophy	9Y
5	23	Female	(1.2, 1.2)	Traumatic CC L. frontal lobe	R. occipital lobe	4Y
6	28	Male	(1.0, 1.0)	CH (R. parietooccipital R. occipital lobe AVM)	R. parietal lobe	4Y
7	41	Male	(1.2, 0.03)	Hypertensive CH	L. temporal lobe	3Y4M
8	33	Male	(1.2, 1.2)	Traumatic DAI	Undetectable	11M

BCVA: best corrected visual acuity; R: right; L: left; PCA: posterior cerebral artery; CC: cerebral contusion; CI: cerebral infarction; AVM: arteriovenous malformation; DAI: diffuse axonal injury; CH: cerebral hemorrhage; Y: year; M: month.

stimuli to shorten the experiment time and developed custom visual field measuring software to make analysis easier (Furuta et al., 2007).

The use of fMRI perimetry would be especially advantageous for the assessment of patients with cerebral lesions. To create objective visual field maps for such patients, measuring brain activation, not retinal response or pupil response, is required. However, fMRI is an indirect measurement method of neural activity via the vascular response. Therefore, a study determining whether fMRI perimetry can be applied to patients with cerebral damage is needed.

In this study, to test the feasibility of fMRI perimetry, we used fMRI to measure 10° of the central visual field in patients with visual field loss caused by cerebral lesions, and compared the results with those of the Humphrey visual field (HVF) test using program 10-2.

Materials and methods

Subjects

Eight patients (mean age ± SD, 38.6 ± 16.0 years; age range, 23–67 years) with visual field defects caused by cerebral lesions served as subjects. A summary of subject data is shown in Table 1.

Visual fields were measured for each eye with the 10-2 program of the HVF analyzer (Carl Zeiss Meditec, Dublin, CA, USA) using the full threshold strategy. In subject 7, HVF was performed on the left eye only, since visual acuity in the right eye was reduced due to glaucoma.

Written informed consent was obtained from each subject after careful explanation of the experiment. The study protocol was approved by the Kanagawa Rehabilitation Hospital Review Board in accordance with the Declaration of Helsinki of the World Medical Association.

Stimuli

The stimuli consisted of an expanding ring moving slowly across the visual field from center to periphery repeatedly (Fig. 1a), and a clockwise (CW) rotating wedge moving after starting from the upper vertical meridian (Fig. 1b). Measurements were made with two additional stimuli—a contracting ring and a counter-clockwise (CCW) rotating wedge (Figs. 1c, d). The loci in the visual field can be expressed with a polar coordinate system (Fig. 1g). For each voxel, the eccentricity can be calculated from averaging the results of the expanding and the contracting ring experiments, and the polar angle can be calculated from averaging the results of the CW and CCW rotating wedge experiments.

To shorten the experiment time, we arranged a CW composite stimulus (Fig. 1e) consisting of the expanding ring and CW rotating wedge, and a CCW composite stimulus (Fig. 1f) consisting of the contracting ring and CCW rotating wedge, cycling at different temporal frequencies.

The stimuli consisted of an 8 Hz black–white reversing dartboard pattern. The cycling periods and size of the stimuli were varied among subjects, since the optimum combination for generating the strongest signals has not yet been determined. For subject 1, a combination of a 27-s period ring with a width 1/4 of the largest radius and a 24-s period rotating wedge with a 45° angular width was used. For subjects 2–8, a combination of a 36-s period ring with a width 1/9 of the largest radius and a 32-s period rotating wedge with a 45° angular width was used. To maintain fixation, subjects were asked to push a button when the color of the fixation point, at the center of the stimuli, changed from red to white every 14.4 s for 0.5 s. The luminance of the white part of the stimuli was 9.7 cd/m^2, and that of the black part was 0.95 cd/m^2. In the background, one white and one black pixel were alternated.

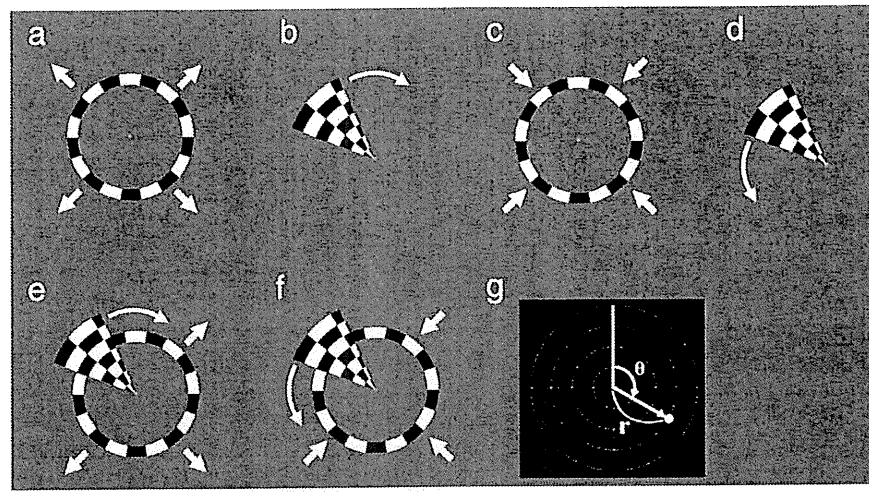

Fig. 1. The visual stimuli presented. (a) Expanding ring stimulus. (b) Clockwise (CW) rotating wedge stimulus. (c) Contracting ring stimulus. (d) Counter-clockwise (CCW) rotating wedge stimulus. (e) CW composite stimulus. (f) CCW composite stimulus. (g) Polar coordinate system. The position on the visual field can be expressed with eccentricity 'r' and polar angle 'θ'.

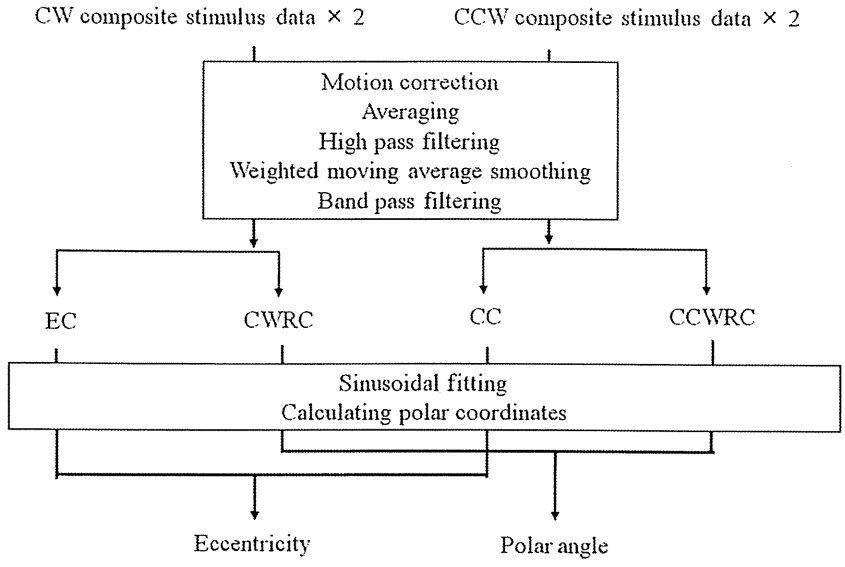

Fig. 2. Flow chart of data analysis. EC, expanding ring component; CWRC, CW rotating wedge component; CC, contracting ring component; CCWRC, CCW rotating wedge component.

The stimuli were presented by a projector (Victor DLA-DS1, Japan) set in the control room, and were projected through the window to an acrylic screen positioned at the subject's feet. Visual stimuli had a maximum 5° visual angle radius. In order to expand the stimulus radius to 10°, the subjects wore non-magnetic 2× magnifying glasses (MAXTV, Eschenbach, Germany). Subjects 1–6 viewed binocularly, while subjects 7 and 8 viewed with the right eye (Table 1). The visual acuity of subject 7 in the left eye was reduced due to glaucoma, and in the case of subject 8, because of binocular diplopia due to exophoria, the left eye was covered during the experiment.

MR experiments

Functional images were acquired using a 1.5 T scanner (Siemens Vision Plus, Erlangen, Germany). Measurement planes were standard single-shot gradient-echo-planar acquisition sequences covering the occipital lobes under the following conditions: parallel to the AC–PC line; voxel size, 3 × 3 × 3 mm; data matrix, 64 × 64; flip angle, 90°; FOV, 192 × 192 mm; 148 volumes (first 4 were discarded). For subject 1, the conditions were: TR, 3 s; TE, 66 ms; slices, 24; experiment time, 444 s. For subjects 2–8, the conditions were: TR, 2 s; TE, 66 ms; slices, 18; experiment time, 296 s. Two experiments each were performed with the CW composite stimulus and CCW composite stimulus. Anatomical images were acquired with a T1-weighted sequence in the same slices.

Data analysis

Fig. 2 shows a flow chart of data analysis. Motion correction was performed using SPM2 (Wellcome Department of Cognitive Neurology, University College London, London, UK). The following analysis was carried out using our custom software for fMRI perimetry, mrFA (Furuta et al., 2007), developed on MatLab 6.5 (MathWorks Inc., Natick, MA, USA). Data from two experiments each were averaged, and then high-pass filtered using a Fourier transform technique at ≤2 Hz. Weighted moving average smoothing was performed using $a(i) = (a(i-1) + a(i) \times 2 + a(i+1))/4$.

The expanding ring component (EC) and the counter-clockwise rotating wedge component (CWRC) were extracted from the CW composite data using band-pass filtering at frequencies equal to, double, and triple the frequency of each other stimulus. Using the same procedures, the contracting ring component (CC) and the CCW rotating wedge component (CCWRC) were extracted from the CCW composite data.

The four components were analyzed by fitting sinusoidal regressors at each stimulus frequency. The highest cross-correlation coefficient and the phase in each voxel were obtained. The eccentricity was calculated from averaging the phases in EC and CC, and the polar angle from averaging the phases in CWRC and CCWRC.

Cortical activations

The active voxels in both EC and CC, in which the threshold of the cross-correlation coefficient was set at 0.37 ($P < 10^{-5}$), were colored corresponding to the eccentricity. Similarly, the active voxels in both CWRC and CCWRC, in which the same threshold was set, were colored corresponding to the polar angle. The active voxels were overlaid on the anatomical images. The correlation threshold was set to 0.37 for all subjects in order to avoid false positive results due to response from the visual field outside the stimulation range.

fMRI visual field maps

A rectangular parallelepiped region of interest (ROI) covering the entirety of the occipital lobes in each subject was set. In the ROI, active voxels (threshold of 0.37, $P < 10^{-5}$) in the EC, CC, CWRW and CCWRW determined on the visual field maps. fMRI visual field maps consist of a voxel-distribution map and a segmented grayscale map. In the voxel-distribution map, active voxels are represented as dots and plotted on the polar coordinate system. The grayscale of each dot reflects the voxel's response strength based on signal amplitude. We set as white any voxels with response strengths above the average value for all voxels plotted, and used a linearly determined grayscale for all voxels with response strengths below this average. In the segmented grayscale map, the visual field was divided into a number of segments, with the response strength in each segment represented in grayscale. To allow for fixation shift, the central visual field within 3° was not divided radially. To set grayscales equally between the periphery, where there are a small number of voxels, and the center, where there are a large number of voxels, the response strength of each voxel in each segment was multiplied by a value reflecting the receptive field area. Here, the size of receptive field was calculated from the following equation (Slotnick et al., 2001):

$$M^{-1} = (E + 0.50)/21.7$$

where M (mm/deg) indicates the cortical magnification factor for V1, and M^{-1} is the inverse magnification. E(deg) indicates the

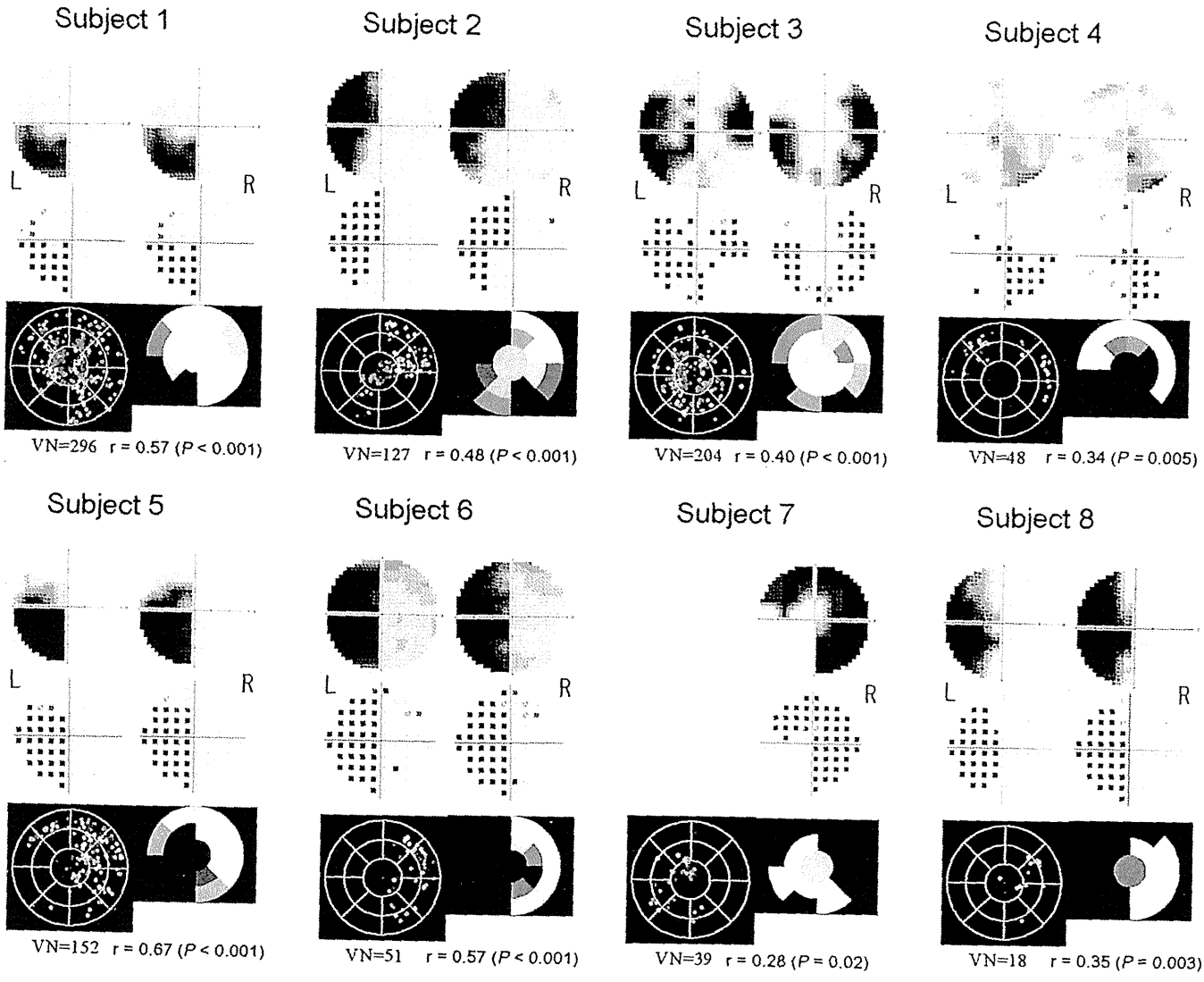

Fig. 4. Visual field maps obtained using HVF and fMRI: HVF grayscale maps (top), pattern deviation plots (middle) and fMRI maps (bottom). VN indicates the number of significantly active voxels used for the visual field maps on fMRI. R, right; L, left; VN, voxel number; r, correlation coefficient.

on fMRI, while fMRI perimetry additionally showed defects in one part of the lower left quadrant that did not agree with HVF. In all other subjects, namely, subjects 1, 5, 6 and 8, there was good agreement between fMRI and HVF, as shown in Fig. 4. In all subjects, resultant correlations were significant at $P<0.05$.

Discussion

In a previous fMRI perimetry study, DeYoe orally reported at the Society for Neuroscience in 2004 that the signals from V1 had been overlaid on HVF in a patient with visual field defects and that the reduction of signals corresponded to the visual field defects. To the best of our knowledge, no further research concerning fMRI perimetry has been reported to date.

The distinctive features of our proposed system are discussed below. First, the use of composite stimuli allows us to reduce experiment time by a half of that using conventional stimuli. Second, with regard to our approach to ROIs, we focus on the entirety of the occipital lobes, not just V1. The area responding to the visual stimuli is not only V1 but also multiple adjacent visual areas in the occipital lobes. To create a visual field map, it is not necessary to identify V1; to set ROIs on the entirety of the occipital lobes is reasonable. In addition, to identify V1 first requires creation of a structural image separating white and gray matter, and because this must be a high-resolution T1-weighted structural image, overall MRI imaging time is further increased. In addition, the work of identifying gray and white matter is mainly manual, and demands time and skill, due in particular to the complex 3-dimensional structure of the occipital lobes. In this regard, our approach of setting the ROIs on the entirety of the occipital lobe is quick and practical. In the occipital lobes, depending on the region, there is a tendency for the area corresponding to the center of the visual field to be large and the area corresponding to the periphery to be small. If we create visual field maps using only the number of activated voxels, the resultant response strength at the center is strong and that at the periphery is weak, and the map is therefore not flat. To create a flat strength map, compensation between the center and the periphery is necessary. As an example, compensation with an arbitrary coefficient being in proportion to eccentricity is useful. In this study, the formula of receptive field size in V1 was expediently used. Because the ROIs in our approach include not only V1 but also plural visual areas, the compensation does not have to employ this formula. However, as a result, this compensation led to the creation of maps similar to the HFAs.

In fMRI, vascular response arising after neural activity is measured as a blood oxygenation level dependent (BOLD) response. In patients with cerebral lesions, a possibility that the vascular response is impaired cannot be excluded. Attenuation of the signal-to-noise ratio and of the BOLD response has been reported in

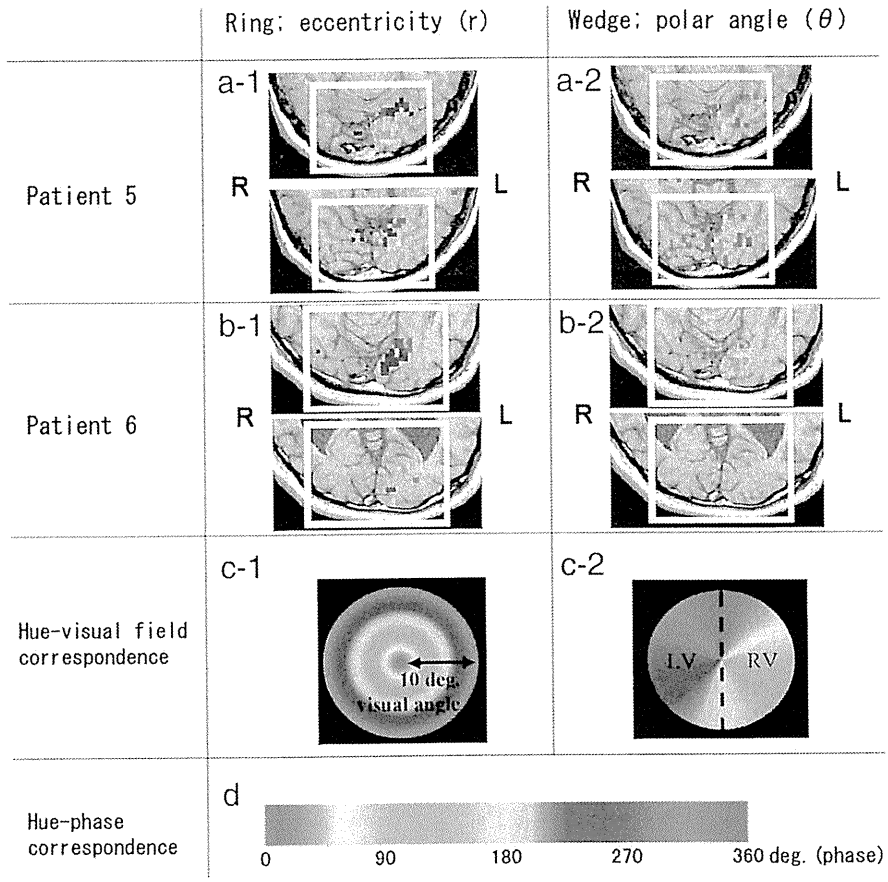

Fig. 3. Correspondence between cortical activations and loci in the visual field. Images (a-1) and (b-1) represent cortical activation with the ring stimuli in subjects 5 and 6, respectively. The color pixels in (a-1) and (b-1) correspond to the color of the visual field in (c-1). Images (a-2) and (b-2) represent the cortical activation with the wedge stimuli in subjects 5 and 6, respectively. The color pixels in (a-2) and (b-2) correspond to the color of the visual field in (c-2). The color reflects phase (degree) as indicated by the color bar (d). The quadrangles covering the occipital lobes are ROIs. HVFs revealed a congruous lower left quadrantanopsia in subject 5, and a congruous left hemianopsia in subject 6, as shown in Fig. 4. In both subjects 5 and 6, pixels in the left occipital lobe responded strongly, while those in the right occipital lobe responded weakly. The color of the active pixels in the posterior part of the occipital lobe (yellow–green) corresponded to the center of the visual field, and that of the active pixels in the anterior part of the medial occipital lobe (blue–purple) corresponded to the periphery of the visual field (a-1, b1). The color of the active pixels in the left occipital lobe (green–yellow–orange) corresponded to the right visual field, and that of the active pixels in the left occipital lobe (purple–red) of subject 5 corresponded to the upper left visual field (a-2, b-2). R, right; L, left; LV, left visual field; RV, right visual field.

eccentricity of the voxel. The product was divided by the segment area to give the response strength for the segment. The grayscale for each segment was determined using the same method as for the voxel-distribution map.

Next, the correlations between visual field maps obtained by HVF and fMRI were calculated. Each voxel-distribution map was segmented with 68 sections corresponding to the measuring points on 10-2 HVF. The total sum of response strengths of voxels in each section was defined as the response strength in the section. The grayscale values were calculated using the same calculations as for the segmented grayscale map. We compared HVFs of the right eye with fMRI. In subject 4, as HVFs of both eyes were not completely congruous and the defects in the left eye were smaller than in the right, HVF of the left eye was used for comparison. Cross-correlation analysis was performed between grayscale values on fMRI and decibel values on HVF.

Results

Cortical activations

Fig. 3 shows the results from two representative subjects. Significant activations in the occipital lobes were observed in all subjects. In the results for the ring stimuli, the color in the posterior part of the occipital lobes corresponded to the center of the visual field, and that in the anterior part corresponded to the periphery. In the results for the rotating wedge stimuli, the color in the right occipital lobe corresponded to the left side of the visual field, and that in the left occipital lobe corresponded to the right side of the visual field. Few or no colored voxels were observed in brain locations that typically represent the visual field defects measured using HVFs (Fig. 4).

Comparison of visual field maps obtained by fMRI and HVFs

Fig. 4 shows visual field maps obtained using fMRI and HVFs. In all subjects (except subject 7), homonymous visual field defects were observed using HVFs. In subject 2, the defects in the upper left quadrant and in one part of the lower left quadrant of the HVFs agreed with the defects on fMRI perimetry, whereas the fMRI additionally showed a wedge-shaped defect in the lower right quadrant that did not agree with HVFs. In subject 3, the defects shown on HVF can be classed as roughly concentric contraction. The segmented voxel-distribution map showed few voxels in the periphery, which was consistent with HVF. In subject 4, the defects in the lower right quadrant on HVF agreed with the defects shown on fMRI. The defects shown on the fMRI, which extended to the lower left quadrant, did not agree with the HVFs. In subject 7, because the optic disc in the right eye had a glaucomatous change, the defects shown on HVF were thought to result from both glaucoma and the cerebral lesion. The right hemifield defects shown on HVF agreed with the defects shown

elderly patients and those with cerebral damage (Bonakdarpour et al., 2007; Huettel et al., 2001; Murata et al., 2006). In our study, there was a significant correlation in all subjects between the fMRI and the HVF. Although this does not mean there was perfect agreement, it is nevertheless of considerable significance that we have been able to demonstrate the feasibility of this system even when patients have cerebral lesions.

The reason for the discrepancy between the HVF and fMRI results is unclear. However, fixation is one possible reason. During the experiment, subjects were asked to focus on a fixation point that changed color. All subjects perfectly performed button-pressing when the color of the fixation point changed; however, it was not possible to confirm whether fixation was satisfactory during the interval between color changes. Fixation is required with fMRI perimetry as it is with subjective perimetry, and the subject's cooperation is therefore necessary.

Visual simulation and imaging parameters used in retinotopic mapping experiments vary among research institutions. In the present study, the parameters used for subject 1 were different from those used for other subjects; after completing the experiment with subject 1, we changed experimental parameters for the subsequent subjects to further shorten the duration of experiment. Results obtained under both conditions were similar to those obtained by subjective perimetry. Thus, even if different parameters are used, correct results can be obtained by analyzing the data appropriately. In future studies, we need to explore the potential for improving testing accuracy by determining the optimal parameters.

As an alternative method of objective perimetry, the usefulness of multifocal visual evoked potentials (mfVEPs) has recently been demonstrated (Kim et al., 2006; Klistorner et al., 2005; Yukawa et al., 2008). This technique requires simpler equipment than fMRI and allows the use of magnetic metals. This technique is reported to be useful due to its applicability even in patients with mental disorders or pediatric epilepsy. fMRI, although not as handy a test method as mfVEPs, is best characterized by its high spatial resolution. fMRI allows for comparison of brain lesions observed on T1-weighted images with brain activity and visual field. For example, patients with visual field defect due to occipital infarction may show gradual restoration of the visual field as periinfarct edema reduces. fMRI may be able to visualize reduction in edema and associated restoration of brain activity at the same region. In patients with cerebral arteriovenous malformation, fMRI may be able to demonstrate the association of reduction in the size of brain lesion following embolization with restoration of brain activity at the same region and visual field. Further, in patients with occipital tumor, preoperatively measuring brain activity around the tumor and the corresponding visual field may help to determine the appropriate resection margin. Although the present study aimed to assess feasibility of using fMRI for objective perimetry, the above-mentioned benefits may be demonstrated in future studies based on the present results.

Finally, we believe that objective perimetry using fMRI has the potential for wider application and we intend to accumulate more cases to further develop the current technique. Without relying on the patient's subjective judgment, this method may aid in the determination of malingering and promises to be useful in patients with, for example, locked-in syndrome, psychogenic visual field disorders, or in unilateral spatial neglect.

Acknowledgments

The authors thank Syuji Maeda, Koshi Maeda, Kunihiro Asakawa, Yoichiro Masuda, Hiroshi Horiguchi, and Shinnichi Yokota for helpful support and discussion.

References

Baseler, H.A., Sutter, E.E., Klein, S.A., Carney, T., 1994. The topography of visual evoked response properties across the visual field. Electroencephalogr. Clin. Neurophysiol. 90, 65–81.
Bearse, M.A.J., Sutter, E.E., 1996. Imaging localized retinal dysfunction with the multifocal electroretinogram. J. Opt. Soc. Am. A. Opt. Image Sci. Vis. 13, 634–640.
Bonakdarpour, B., Parrish, T.B., Thompson, C.K., 2007. Hemodynamic response function in patients with stroke-induced aphasia: Implications for fMRI data analysis. NeuroImage 36, 322–331.
Duncan, R.O., Sample, P.A., Weinreb, R.N., Bowd, C., Zangwill, L.M., 2007. Retinotopic organization of primary visual cortex in glaucoma: comparing fMRI measurements of cortical function with visual field loss. Prog. Retin. Eye. Res. 26, 38–56.
Engel, S.A., Rumelhart, D.E., Wandell, B.A., Lee, A.T., Glover, G.H., Chichilnisky, E.J., Shadlen, M.N., 1994. fMRI of human visual cortex. Nature 369, 525.
Engel, S.A., Glover, G.H., Wandell, B.A., 1997. Retinotopic organization in human visual cortex and the spatial precision of functional MRI. Cereb. Cortex 7, 181–192.
Furuta, A., Nakadomari, S., Misaki, M., Miyauchi, S., Kitahara, K., 2007. The objective visual field map using functional magnetic resonance imaging with hemi field visual stimulus. Jpn. J. Neuro-Ophthalmol. 24, 316–326.
Huettel, S.A., Singerman, J.D., McCarthy, G., 2001. The effects of aging upon the hemodynamic response measured by functional MRI. NeuroImage 13, 161–175.
Kardon, R.H., Kirkali, P.A., Thompson, H.S., 1991. Automated pupil perimetry: pupil field mapping in patients and normal subjects. Ophthalmology 98, 485–495.
Kim, Y.J., Yukawa, E., Kawasaki, K., Nakase, H., Sakaki, T., 2006. Use of multifocal visual evoked potential tests in the objective evaluation of the visual field in pediatric epilepsy surgery. J. Neurosurg. 104 (3 Suppl.), 160–165.
Klistorner, A.I., Graham, S.L., Grigg, J., Balachandran, C., 2005. Objective perimetry using the multifocal visual evoked potential in central visual pathway lesions. Br. J. Ophthalmol. 89, 739–744.
Kollias, S.S., Landau, K., Khan, N., Golay, X., Bernays, R., Yonekawa, Y., Valavanis, A., 1998. Functional evaluation using magnetic resonance imaging of the visual cortex in patients with retrochiasmatic lesions. J. Neurosurg. 89, 780–790.
Lee, Y.J., Chung, T.S., Yoon, Y.S., Lee, M.S., Han, S.H., Seong, G.J., Ahn, K.J., 2001. The role of functional MR imaging in patients with ischemia in the visual cortex. AJNR Am. J. Neuroradiol. 22, 1043–1049.
Murata, Y., Sakatani, K., Hoshino, T., Fujiwara, N., Kano, T., Nakamura, S., Katayama, Y., 2006. Effects of cerebral ischemia on evoked cerebral blood oxygenation responses and BOLD contrast functional MRI in stroke patients. Stroke 37, 2514–2520.
Nishiyama, T., Ohde, H., Haruta, Y., Mashima, Y., Oguchi, Y., 2004. Multifocal magnetoencephalogram applied to objective visual field analysis. Jpn. J. Ophthalmo. 48, 115–122.
Sereno, M.I., McDonald, C.T., Allman, J.M., 1994. Analysis of retinotopic maps in extrastriate cortex. Cereb. Cortex 4, 601–620.
Slotnick, S.D., Klein, S.A., Carney, T., Sutter, E.E., 2001. Electrophysiological estimate of human cortical magnification. Clin. Neurophysiol. 112, 1349–1356.
Tootell, R.B., Dale, A.M., Sereno, M.I., Malach, R., 1996. New images from human visual cortex. Trends Neurosci. 19, 481–489.
Wandell, B.A., Wade, A.R., 2003. Functional imaging of the visual pathways. Neurol. Clin. 21, 417–443.
Wandell, B., Chial, S., Backus, B.T., 2000. Visualization and measurement of the cortical surface. J. Cogn. Neurosci. 12, 739–752.
Wong, A.M.F., Sharpe, J.A., 1999. Representation of the visual field in the human occipital cortex: a magnetic resonance imaging and perimetric correlation. Arch. Ophthalmol. 177, 208–217.
Yukawa, E., Matsuura, T., Kim, Y.J., Nitta, N., Taketani, F., Hara, Y., 2008. Objective visual field evaluation using multifocal visual evoked potentials in patients with intracranial disease complicated by mental disorders. Clin Neurol Neurosurg. 110, 592–598.

Vitreous Mediators after Intravitreal Bevacizumab or Triamcinolone Acetonide in Eyes with Proliferative Diabetic Retinopathy

Noboru Arimura, MD,[1] Hiroki Otsuka, MD,[1] Keita Yamakiri, MD, PhD,[1] Yasushi Sonoda, MD,[1] Shintaro Nakao, MD, PhD,[2] Yoshihiro Noda, MD, PhD,[2] Teruto Hashiguchi, MD, PhD,[3] Ikuro Maruyama, MD, PhD,[3] Taiji Sakamoto, MD, PhD[1]

Purpose: To evaluate vitreous vascular endothelial growth factor (VEGF), stromal cell-derived factor 1α (SDF-1α), interleukins (ILs), and tumor necrosis factor-α (TNF-α) after intravitreal bevacizumab or triamcinolone acetonide (TA) in eyes with proliferative diabetic retinopathy (PDR).

Design: Interventional, consecutive, retrospective, comparative study with a historical control.

Participants: Forty-seven eyes of 47 patients affected by active PDR were investigated. Bevacizumab (1.25 mg; 19 eyes; bevacizumab group) or TA (4 mg; 10 eyes; TA group) was injected into the vitreous cavity as preoperative adjunctive therapy 7 days before vitrectomy. Eighteen eyes without injection served as controls (control group).

Methods: The vitreous samples were obtained at vitrectomy and were analyzed for concentrations of total protein, VEGF, SDF-1α, IL-1β, IL-6, IL-8, IL-10, IL-12p70, and TNF-α.

Main Outcome Measures: Vitreous concentrations of VEGF, SDF-1α, ILs, and TNF-α were compared among bevacizumab, TA, and control groups.

Results: Vitreous concentrations of VEGF and SDF-1α were lower in bevacizumab and TA groups compared with the control group. The median VEGF level was 0 pg/ml (range, 0–79.2 pg/ml) in the bevacizumab group, 343.5 pg/ml (range, 0–1683.3 pg/ml) in the TA group, and 1202.5 pg/ml (range, 76–4213.9 pg/ml) in the control group. The median SDF-1α level was 149.2 pg/ml (range, 0–519.4 pg/ml) in the bevacizumab group, 87.5 pg/ml (range, 0–252.5 pg/ml) in the TA group, and 245.7 pg/ml (range, 0–856.8 pg/ml) in the control group. The differences in both vitreous VEGF and SDF-1α concentrations among 3 groups were statistically significant ($P<0.001$ and $P = 0.010$, respectively). The eyes with intravitreal bevacizumab demonstrated the lowest vitreous level of VEGF, and the level was statistically significant compared with the eyes with intravitreal TA and control eyes ($P<0.001$ and $P<0.001$, respectively). The control eyes had the highest vitreous level of SDF-1α, and the level was statistically significant compared with the eyes with intravitreal bevacizumab and TA ($P = 0.015$ and $P = 0.009$, respectively). There was no significant difference regarding ILs and TNF-α.

Conclusions: Intravitreal injection of bevacizumab potentially diminishes not only VEGF but also SDF-1α. These findings suggest that intravitreal bevacizumab may influence intraocular mediators beyond VEGF.

Financial Disclosure(s): The author(s) have no proprietary or commercial interest in any materials discussed in this article. *Ophthalmology 2009;116:921–926*

Various angiogenesis inhibitors have been developed for angiogenesis-dependent diseases including ocular neovascular disorders.[1] In particular, vascular endothelial growth factor (VEGF) inhibitors, including bevacizumab, have been applied increasingly for the treatment of ocular pathologic angiogenesis because of their potent antiangiogenic and antipermeability effects. Triamcinolone acetonide (TA), one of the angiostatic corticosteroids, also has been used primarily for the treatment of intraretinal edema because of its strong anti-inflammatory and antipermeability properties. Despite some controversy over their use, bevacizumab[2,3] and TA[4] both have been accepted for clinical use in the treatment of age-related macular degeneration, diabetic retinopathy, and retinal vein occlusion.

Previous studies indicate that intraocular administration of TA results in dramatic reductions of VEGF and stromal cell-derived factor 1 (SDF-1) in patients with diabetic retinopathy[5] and that intravitreal injection of bevacizumab also diminishes intraocular VEGF dramatically in diabetic retinopathy.[6] Vascular endothelial growth factor is a central factor that orchestrates angiogenesis, which is regulated partially by inflammation. Triamcinolone acetonide is a potent drug with an anti-inflammatory property. Consequently, the authors hypothesized that intravitreal bevacizumab and TA may cause some alteration of proangiogenic and inflammatory mediators in the eye. As far as the authors are aware, data from this viewpoint have been limited. Conversely, intravitreal administrations of these antiangiogenic agents have spread widely in the treatment of ocular

ISSN 0161-6420/09/$–see front matter
doi:10.1016/j.ophtha.2008.12.024